Hierarchical MPC for Energy Management of Multi-Energy Systems

Case Study Based on a Power-to-X Concept

Oğuzhan Kaya

Master of Science Thesis

TU Delft Delft University of Technology

Delft Center for Systems and Control

Hierarchical MPC for Energy Management of Multi-Energy Systems

Case Study Based on a Power-to-X Concept

Master of Science Thesis

For the degree of Master of Science in Systems and Control at Delft University of Technology

Oğuzhan Kaya

February 8, 2020

Faculty of Mechanical, Maritime and Materials Engineering (3mE) · Delft University of Technology

KWR Watercycle Research Institute supported the work in this thesis. Their cooperation is hereby gratefully acknowledged.

Abstract

All over Europe, the expansion of renewable energy sources is quickly proceeding, fueled by environmental and political motives. The power generated by renewables is heavily subject to the intermittency of the source, e.g. the availability of wind or solar irradiance. Consequently, electrical grids that rely on renewable sources alternate between periods of excess power availability and periods with lack of power production. Excess power is often curtailed or exported, whereas the shortage of power production must be imported or produced through the deployment of more expensive production units.

Power-to-X strategies aim to utilise the excess power from renewables more effectively, by converting power to another energy carrier within the grid, e.g. heat or hydrogen. By allowing the transition of power to another energy carrier, the system is transformed into a so-called multi-energy system. Therefore, the system takes into account the multiple energy carrier's system characteristics and loads in an integrated way. This formulation allows for optimal scheduling of energy flows in the system while taking into account characteristics of each energy carrier, e.g., storage characteristics, time-varying costs or production emissions.

The main focus of this thesis to deal with the tasks of an energy management system for the aforementioned system using Model Predictive Control. The Model Predictive Control framework allows real-time optimal scheduling while incorporating data-driven forecasts of future loads and generation in the grid. Due to the stochastic nature of these forecasts, this thesis also looks into extensions of Model Predictive Control that can cope with uncertainties. Furthermore, to handle the different timescales of the grid dynamics, Model Predictive Control for multi-timescale systems is investigated. In particular, the performance of a Heuristic Model Predictive Control scheme and a Hierarchical Model Predictive Control scheme on the control of a simulated Power-to-X based energy system are compared. The simulation is based on a conceptual Power-to-X system based on historical data of the Dutch energy sector. Based on this case study, a statement is made about the suitability of the Power-to-X principles to future Dutch sustainable neighbourhoods. Moreover, a statement regarding the economic viability of the presented concept is made based on the simulations.

Table of Contents

Acknowledgements

First and foremost, I wish to show my gratitude to my supervisor Dr.ir. T. Keviczky who has guided and encouraged me throughout this long journey. His professional feedback and eye for detail have helped me in successfully completing my thesis. I would also like to thank my daily supervisors at KWR, Els van der Roest MSc and Dr.ir. Dirk Vries for the opportunity to work on an inspiring project. Their immense support, detailed feedback and meaningful meetings have helped me during the course of my thesis. Also, special thanks to my friend Ridvan Karagoz for proofreading this thesis.

Moreover, I wish to express my gratitude to my parents for providing me with their support and encouragement throughout my years of study. Last but not least, I want to express my gratitude towards my wife, Melda, who has stood by me through all my travails, my absences, my fits of impatience. This accomplishment would not have been possible without you. Thank you.

Delft, University of Technology
February 8, 2020

Oğuzhan Kaya

Chapter 1

Introduction

The Paris Climate Agreement is a collective effort of more than 190 countries to take measures to counter global climate change. One of its main goals is to keep the global average temperature increase to well below 2 degrees Celsius above 'pre-industrial' levels [1]. The Paris Climate Agreement and other European agreements shape the national policies of European countries, including the Netherlands. The coalition agreement of the Third Rutte cabinet, formed after the Dutch general elections of 2017 states, that the Netherlands must reach the goals set in the Paris Climate Agreement. The national targets of the Netherlands also state that emissions of greenhouse gasses should be reduced by 49% in 2030 compared to 1990 [2]. The transition from fuel-based energy generation (e.g. coal and diesel) to Renewable Energy Sources (RESs) (e.g. photovoltaic (PV) and wind generation) is expected to contribute to a reduction of 17 Mt of CO_2 in 2030 [2].

In general, residential energy consumption may be divided into *electrical* energy, *thermal* energy, and energy for *mobility*. The electrical energy demand is traditionally met through centralised power infrastructures, where transmission and distribution lines provide connections between large power plants and residential areas. With the steadily increasing demand for energy and the increasing penetration of RESs, the traditional electricity infrastructures make space for distributed generation solutions, see Figure 1-1. These developments are also possibly caused by the shift from monopolistic frameworks to liberalised markets, which provide open access for various (new) participants and introduce benefits for multiple stakeholders [4]. When a local distribution grid is transformed into an active network, this system is called a **microgrid** [5]. Microgrids have proven to be quite effective for the implementation of RESs in the grid. The microgrid allows for interconnecting multiple local distributed power generation and loads, which makes them highly suitable for control [5]. However, due to the intermittent generation of power from RESs, many microgrids still rely on the use of backup fossil fuel generators. This increase of RESs in the grid means that the generation of power is dominated by uncertain weather forecasts and seasonal generation discrepancies. Recently, in Germany, consumers in the electricity market were paid to use electricity because wind generation created more output than needed [6]. Furthermore, in the case of PV generation, apart from the day and night differences, surplus power is generated in the summer, where less power is generated in the winter.

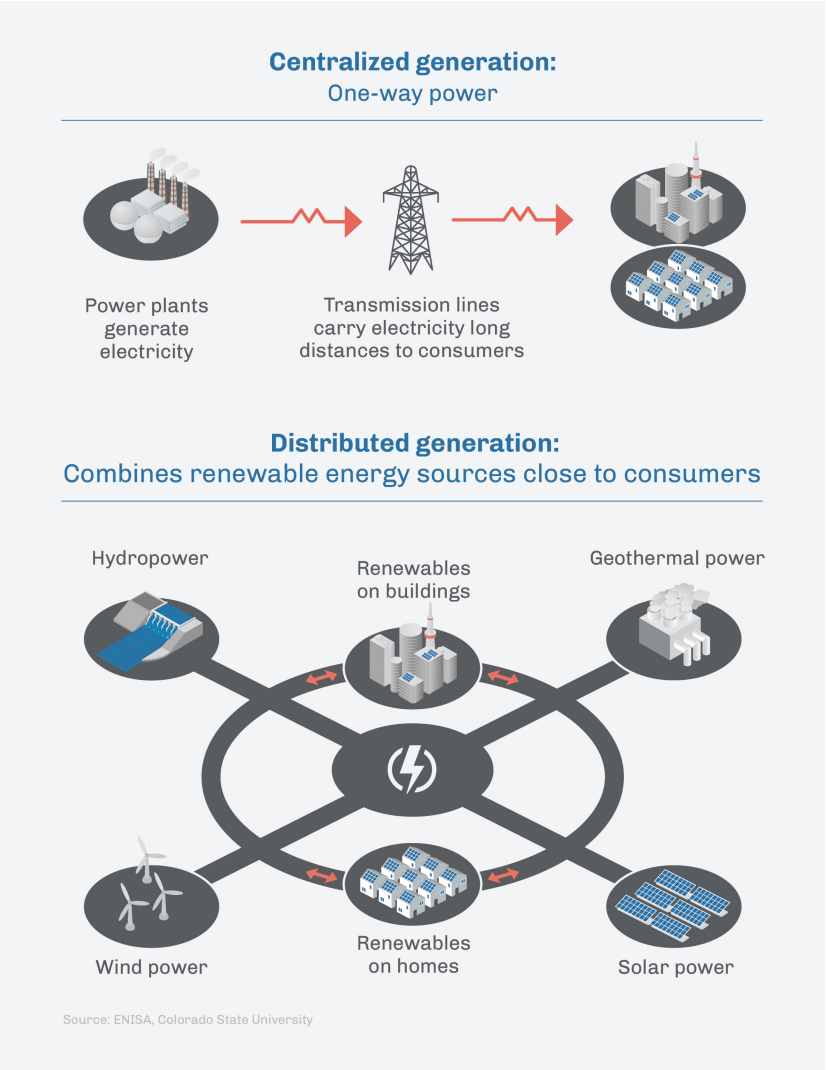

Figure 1-1: Centralised and distributed generation in power infrastructures [3].

Formally, surplus electricity production (SEP) is defined by the authors of [7] as situations in which electricity production exceeds the demand in a given area. Surplus production, which can be exported, is defined as exportable surplus electricity production (ESEP). Lately, a designated power line for the export of the surplus 'green' energy from Germany to the Netherlands has been established [8]. However, in the near future when the Netherlands increases its share of RES generation, a scenario could occur where the surplus electricity cannot be exported due to operational or economic limitations.

Fueled by the need to reduce greenhouse gas emissions to mitigate the effects of global climate changes and political factors, it is of great importance to utilise surplus energy from RESs optimally. One solution investigated in this thesis is Power to X. Generally, Power to X refers to the utilisation of surplus energy from RESs. Here, X stands for the energy service to which this excess is converted to, e.g. thermal energy, hydrogen, gas or mobility [9]. Furthermore, Power to X refers to conversion that allows for the decoupling of power from the electricity sector for use in other sectors. Systems that take into account several energy sectors as a

whole are referred to as Multi-Energy Systems (MESs) [10] or multi-carrier systems. The integration of multiple energy carriers may increase the system's reliability, load flexibility and provide synergy effects [11].

1-1 Power to X: Motivation

As mentioned before, traditionally, the operation and planning of energy sectors (e.g. electricity, heating, gas, and mobility) have been decoupled. However, many interactions between these sectors are already present in the form of co- and tri-generation, e.g. combined heat pump technologies, electric heat pumps and so on [12]. These systems combine several energy carriers such as electricity, thermal energy, natural gas, etc. Coordinating these energy carriers in an integrated way may result in a vital aspect for cleaner and more efficient energy systems, which are called MESs [10]. Potential benefits of the integration of multiple energy carriers may be [10, 11]:

- **Increased Reliability:** Considering multiple inputs which can be used to meet output demand of a particular energy carrier makes it clear that integrated energy structures increase reliability by increasing the availability of the energy for that load;
- **Increased Load Flexibility:** Several different input paths may supply certain energy loads. For instance, the demand for electricity may be met by consuming power from the corresponding input. However, it may also be supplied by combusting natural gas in a gas turbine. Depending on the availability, or the energy tariffs at a specific time one or the other may be more attractive to utilise, from a system point of view;
- **Optimisation Potential:** The fact that various inputs and different combinations of them can be used to meet the output requirement yields to the question of optimal supply. The different inputs can be characterised by different costs, related emissions, availability, and other criteria. Therefore, the system's operation is highly suitable to be solved as an optimisation problem;
- **Synergy Effects:** The MES consists of different energy carriers, each showing specific characteristics. Electricity, for example, can be transmitted over long distances with comparably low losses. However, generally, electricity is only stored in the order of hours to weeks. Thermal energy or hydrogen, however, can be stored over multiple seasons. Several characteristics of various energy carriers can be combined to provide desired synergy effects.

Furthermore, the increase of RES in the power grid and their intermittent generation caused problems related to grid operation and planning [13]. On the one hand, supply flexibility is required to counter limited RES predictability to cover short-term deviations from the forecasted feed-in schedule. For example, units capable of responding quickly to changes in residual loads are battery energy storage system (BESS) units and gas-fired power plants. On the other hand, RES production is subject to seasonality, for instance, PV generation differences in winter and summer. During specific periods, excess energy from RES is curtailed or exported, while during periods of lack of production, more expensive units are deployed to produce electricity.

Power to X is the family of technologies regarding the utilisation of the surplus energy produced from RES during periods where excess is available. The following Power to X solutions are the current field of interest for many research papers:

- **Power to Heat:** Focuses on converting excess energy to heat, which could either be stored or consumed [14, 15]. Power to heat may bridge the seasonal difficulties RES generation faces since highly effective seasonal thermal storage units exist [16]. Generally, electrical heat pumps are considered to be the link between electrical power and heat generation;
- **Power to Gas:** In the power-to-gas approach excess energy is converted into gas products [13, 17], i.e. hydrogen or methane, see Figure 1-2. Gas products are generally highly suitable for seasonal storage purposes due to their relatively large storage capacity, see Figure 1-3 where multiple storage technologies are compared in terms of their discharging rates and typical capacity. Subsequently, gas products may benefit from already existing gas transportation networks, saving both operational and investment costs [13, 18]. Furthermore, with the use of fuel cells, hydrogen can be used to shift excess energy to periods of shortage and thereby contribute to the power supply. Reusing hydrogen for example for electricity supply, mobility (e.g. hydrogen vehicles) or chemical industrial purposes is called hydrogen-to-X [19];
- **Power to Mobility:** May refer to utilising power for the mobility of vehicles, e.g. electric or hydrogen. Power to Mobility may result in an overlap with power-to-gas or power-to-power systems. An interesting scenario arises when vehicles are allowed to contribute to the grid's power balance, resulting in vehicle-to-grid systems [20, 21];
- **Power to Power:** Occurs, for instance, when excess power is stored in batteries or capacitors.

Note that, in this work, Power to X as a family of the techniques above is used interchangeably with the fact that multiple techniques could exist in a single Power-to-X system. Subsequently, in this work, a Power-to-X system is viewed as an MES. In Chapter 2, the Power-to-X system considered in this work will be further elaborated.

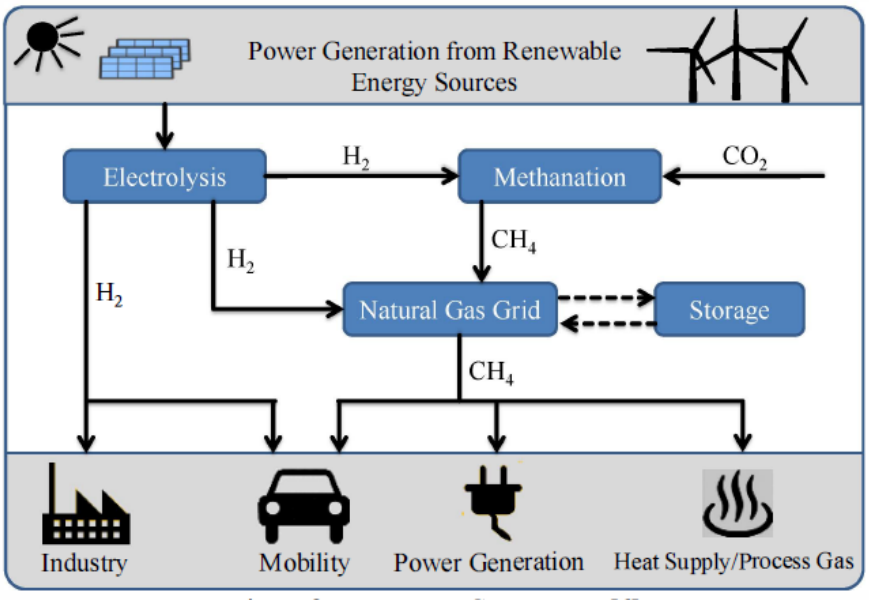

Figure 1-2: Typical power-to-gas system based on methane and hydrogen, very obvious is the fact that this system is unwittingly also a power-to-mobility and power-to-heat system [17].

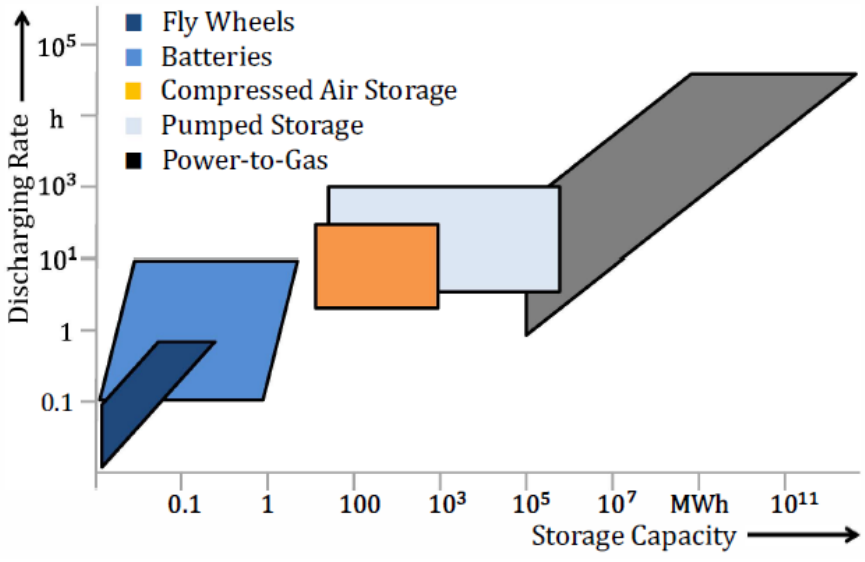

Figure 1-3: Energy storage potential presented as discharging rate vs. storage capacity [13].

1-2 Power to X: Challenges

Practically all Power-to-X systems consist of multiple RESs, storage elements, and conversion units. The energy flows within the system are determined by the Energy Management System (EMS) taking into account multiple technical and economic considerations. EMSs for Power-to-X systems may have to make decisions about:

- How much of a particular energy carrier should be generated/produced to meet that energy carriers load at minimum economic or environmental cost (energy dispatch);
- When each generation unit should be started and stopped (unit commitment);
- Whether and how much of a certain energy carrier is exchanged with an external party, e.g. the utility grid;
- How much of a particular energy carrier is stored or taken from the corresponding storages, taking into account seasonal differences.

In recent literature, Model Predictive Control (MPC) had already gained attention for energy management purposes in power systems. This popularity arose mainly due to its ability to easily integrate predictions, system constraints and decision making based on feedback [22]. MPC solves an optimal control problem with the desired goal as objective function and system inputs as its decision variables. The system dynamics are predicted N steps ahead with a prediction model. The first input vector of the computed sequence of N input vectors is applied. Next, the system states are measured and the procedure is repeated. Relevant theoretical background on MPC will be introduced in Chapter 2. MPC for energy management of Power-to-X systems is mainly subject to challenges regarding the computational complexity from the prediction horizon and stochastic behaviour of uncertainties acting on the system, such as uncertain RES generation or demand profiles.

1. **Computational Complexity:** The computational complexity of the optimal control problem is mainly dominated by the number of system inputs and the prediction horizon N. Since we are dealing with seasonal discrepancies in demand and generation in Power-to-X systems we should formulate an optimal control problem that is able to capture these seasonal differences in the prediction, see Figure 1-4. This can be achieved by increasing the prediction horizon; however, if we are dealing with a system with an hourly sampling interval the complexity of the system has gone far beyond tractability. Relevant literature has proposed a move-blocking scheme [23] or multi-layered control schemes [24, 25], i.e. Hierarchical Model Predictive Control (HiMPC).
2. **Dealing with Uncertainties:** The deterministic framework is the most straightforward framework of MPC. The main assumption of this framework to cope with uncertainties relies on the so-called certainty-equivalence property [26]. In general, this means that imperfect load and weather forecasts are assumed to be correct, i.e. which in the case of the MPC framework results in a perturbed nominal MPC controller [22, 26–29]. On the contrary, the stochastic MPC framework includes probabilistic information on the uncertain variables in the optimal control problem formulation. In real applications, it might not be practical to use this approach because it is not trivial to know the probabilistic distribution beforehand. Nevertheless, historical data may form a sound basis for scenario-based MPC in a stochastic setting.

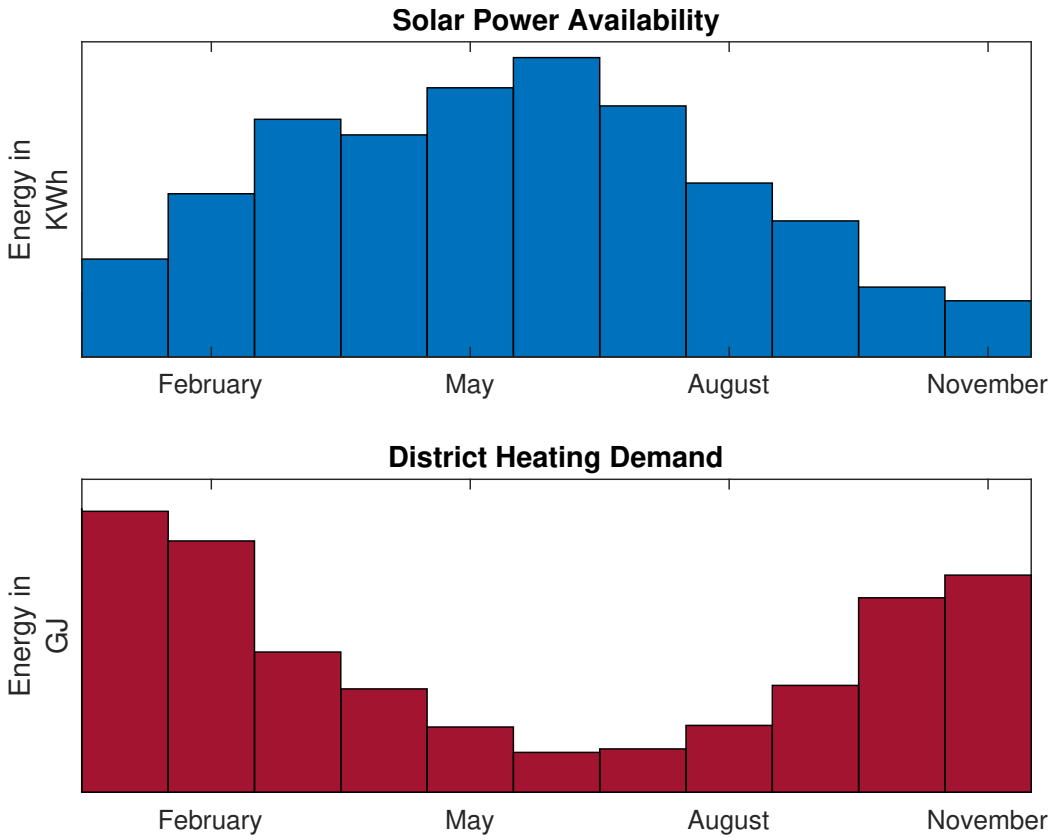

Figure 1-4: Temporal mismatch of energy availability and energy demand.

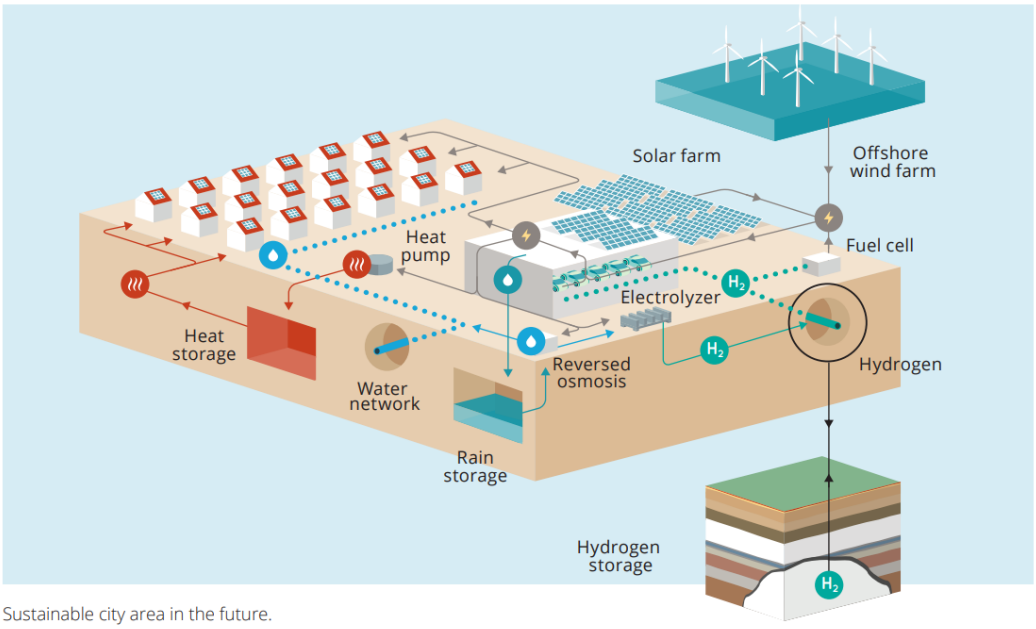

Figure 1-5: Power-to-X system as conceptualised by KWR, including electricity, heat, hydrogen and (demineralised) water supply, demand and generation [30].

1-3 Research Objectives

This research is concerned in giving insight into the economic viability of a Power-to-X system incorporated in the present-day grid subject to suitable MPC frameworks, namely deterministic and stochastic. This study will contain a case study on a Power-to-X system concept of KWR, see Figure 1-5. Though, the work conducted in this thesis should be widely applicable for microgrids, MES, and other Power-to-X configurations than the presented case study.

1-4 Thesis Contribution

The main contributions of this thesis are presented below:

1. Performed a case-study on the viability of MPC as the EMS of a Power-to-X system concept consisting of electricity, thermal energy, hydrogen, and water. MPC in a deterministic and stochastic framework using real datasets are compared in this case study.
2. Proposed, tuned, and assessed the performance of the following three MPC formulations for Power-to-X systems:
   (a) **Heuristic Model Predictive Control (HMPC)**: An economic-MPC including heuristic terminal cost assignment resulting in a single-layer control framework for MPC for Power-to-X systems;
   (b) **HiMPC**: A two-layer control framework consisting of two separate economic-MPC problems for different time-scales. Two variants are proposed for controller interactions, one based on linear interpolation variant and another with a heuristic reference assignment.
3. Proposed a control-oriented Mixed Logical Dynamical (MLD) model for Aquifer Thermal Energy Storage (ATES) systems integrated as seasonal heat storage in district heating networks based on thermal energy only.

1-5 Thesis Outline

This thesis consists of five chapters which are ordered as such:

Chapter 2 discusses the system components and relevant subsystems of the Power-to-X concept as conceptualised by KWR. Control-oriented models will be presented, accompanied by a relevant theoretical background on hybrid systems modelling. The exogenous disturbances acting on the system will be analysed, and forecasting will be discussed.

Chapter 3 introduces relevant MPC frameworks for MPC of any Power-to-X system, including HMPC, HiMPC, and the deterministic and stochastic-MPC (SMPC) frameworks. The mathematical formulations of MPC optimal control problems will be presented for the current case study. However, these MPC formulations are meant to be easily applicable for any Power-to-X concept design.

Chapter 4 provides a detailed approach to the simulation choices and relevant assumptions of the proposed controllers in Chapter 3 and presents appropriate tuning methods applied to these controllers. Then, based on these simulations, controllers will be assessed and compared based on performance indices.

Chapter 5 is the concluding chapter of this thesis, including a summary, concluding remarks, recommendations and future work.

Chapter 2

System Description and Modelling

2-1 Introduction

Control theory mainly focuses on systems whose state transitions are described by smooth linear or nonlinear state transformation functions. For Model Predictive Control (MPC), these models are used to predict future states in an open-loop optimal control fashion [22]. The choice of the modelling structure of the dynamic system is influenced by the physical system properties and dynamic behaviour, coupled with the intended control application in mind. Generally, there exists a trade-off between capturing the system's dynamics as detailed as possible versus keeping computational effort low. Consider the general continuous-time dynamical system given by:

$$\dot{x}(t) = f_{\mathrm{c}}(x(t), u(t), \omega(t)), \tag{2-1}$$

where t indicates the time, $x(t) \in \mathbb{X} \subseteq \mathbb{R}^n$, $u(t) \in \mathbb{U} \subseteq \mathbb{R}^m$ and $\omega(t) \in \mathbb{W} \subseteq \mathbb{R}^w$, represent the state vector, manipulated input vector and disturbance vector respectively.

While continuous-time dynamics generally govern real-world physical systems, control techniques are usually deployed through computers. Hence this thesis focuses on discrete-time system models. In the next chapters, the reader may assume that the presented discrete-time systems were achieved through zero-order-hold discretisation unless stated otherwise. Subsequently, the generic discrete-time state-space model is governed by general difference equations of the form:

$$x(k+1) = f_{\mathrm{d}}(x(k), u(k), \omega(k)), \tag{2-2}$$

where $x(k) \in \mathbb{X} \subseteq \mathbb{R}^n$, $u(k) \in \mathbb{U} \subseteq \mathbb{R}^m$, $\omega(k) \in \mathbb{W} \subseteq \mathbb{R}^w$, denote discrete-time state vector, manipulated input vector and disturbance vector respectively. Typically the input vector $u(k)$ is constrained by the available control energy indicated by the set $\mathbb{U}$. Furthermore, the disturbance vector $\omega(k)$ may include modelling errors, uncontrollable exogenous inputs, and unknown external forces and is assumed to be bounded by the disturbance set $\mathbb{W}$. Furthermore, index k denotes the discrete-time instant.

Hybrid systems are systems constituted by both continuous-valued and discrete-valued variables. The states of hybrid systems are governed by equations of motion that contain mixtures

of logic and discrete-value dynamics and continuous-variable dynamics [31]. These systems have been proven to be useful for accurately representing systems with distinct modes, such as charging/discharging in batteries, on/off modes for generators and heating/cooling in thermal energy storages. In literature there exist multiple subclasses of hybrid dynamical systems. Some examples of such systems are Piecewise-Affine (PWA) systems [32], Mixed-Logical-Dynamical (MLD) systems [33] and Linear-Complementarity (LC) systems [34]. Each of these subclasses may have its advantage over the others. This thesis will mainly focus on PWA and MLD systems because stability criteria were proposed for PWA systems [35] and control and verification techniques exist for MLD hybrid models [33]. In past literature, the equivalence of several subclasses of hybrid systems has been proven under mild assumptions [36]. These results are important because the individual analysis and synthesis tools of each subclass can be applied to any of the equivalent subclasses of the hybrid modelling framework.

PWA Systems

PWA systems have been considered by several authors to form the 'simplest' extension of linear systems that can capture non-linear and non-smooth processes with arbitrary accuracy in the hybrid modelling framework [36]. PWA systems are described by [32]:

$$\begin{aligned} x(k+1) &= A_i x(k) + B_i u(k) + f_i \\ y(k) &= C_i x(k) + D_i u(k) + g_i \end{aligned} \qquad \text{for} \begin{bmatrix} x(k) \\ u(k) \end{bmatrix} \in \Omega_i, \tag{2-3}$$

for $i = 1, \ldots, V$ where $\Omega_1, \ldots, \Omega_V$ are convex polyhedra (i.e. given by a finite number of linear inequalities) in the input/state space with non-overlapping interiors.

MLD Systems

MLD systems were first introduced by Bemporad et al. in [33] as a class of hybrid systems in which logic, dynamics and constraints are integrated. MLD systems are described by:

$$x(k+1) = Ax(k) + B_1 u(k) + B_2 \delta(k) + B_3 z(k), \tag{2-4a}$$

$$y(k) = Cx(k) + D_1 u(k) + D_2 \delta(k) + D_3 z(k), \tag{2-4b}$$

$$E_1 x(k) + E_2 u(k) + E_3 \delta(k) + E_4 z(k) \leq g_5, \tag{2-4c}$$

where $x(k)$ is the state vector containing both real and binary-valued states ($y(k)$ and $u(k)$ have similar structures), and where vectors $z(k)$ and $\delta(k)$ contain real and binary auxiliary variables, respectively.

2-2 Case Study: Power-to-X System Description and Elements

The case-study studied in this thesis originates from a concept of KWR's sustainable city area in the future [30]. This concept is a Power-to-X system sized to supply a neighbourhood of its electricity, heating, hydrogen and water demands, see Figure 1-5. The underlying electrical system is a grid-connected microgrid consisting of Renewable Energy Sources (RESs) and a battery energy storage system (BESS). Contrary to the concept depicted in Figure 1-5 the case-study considered in this thesis is slightly adjusted. The energy flowchart of the adjusted concept is shown in Figure 2-1. These elements in the diagram are described in Table 2-1.

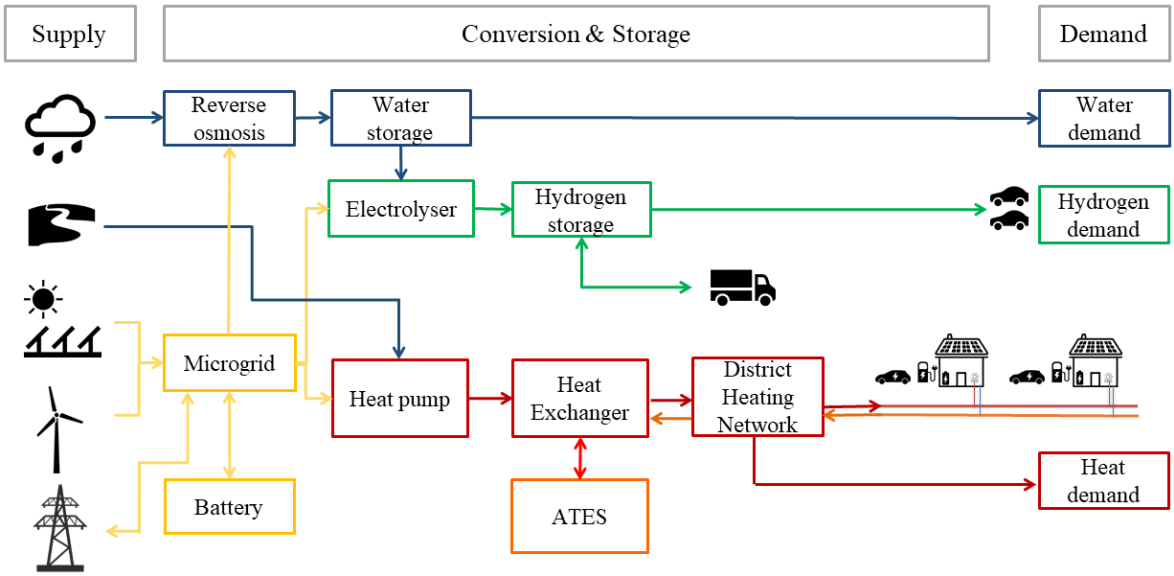

Figure 2-1: Schematic energy flow diagram of the Power-to-X system. Energy flows in yellow correspond to electricity, blue to water, and green and red to hydrogen and heat, respectively.

The remainder of this section provides a description and mathematical model of all the subsystems of the Power-to-X system. These subsystems are the microgrid, district heating network and hydrogen and water utilities. For each of these subsystems, the components will be elaborated and dynamical storage models will be presented. From this point on vectors are denoted with bold style, e.g. $\boldsymbol{x}$ and scalars with non-bold text style. Furthermore, the generic discrete-time instant is denoted by k and τ is the sampling time.

Technology	Principle	Description
Conversion		
Heat Pump	Power to Heat	Converting power to heat by extracting heat from a source, e.g. water.
Electrolyser	Power to Gas	Generating hydrogen from water using power for an electrolyser.
Reverse Osmosis	Power to Water	Purifying rainwater for residential consumption.
Storage		
BESS	Power to Power	Quickly dispatchable short-term electricity storage.
Aquifer Thermal Energy Storage (ATES)	-	Long term storage element for storing thermal energy underground in porous formations.
Hydrogen Tank	-	Storing large quantities of hydrogen for a short amount of time.
Water Tank	-	Large capacity storage of purified rainwater.

Table 2-1: Power-to-X system elements, principles and description.

2-2-1 Microgrid

The power system under study in this thesis consists of a neighbourhood-sized microgrid whose energy is generated by a local solar farm. For this work, we assume that no power is curtailed from RES generation and any surplus energy can be either converted into another energy sector or stored in a BESS. Furthermore, the microgrid operates in grid-connected mode, which makes electricity exchange between the system and the utility grid possible.

Battery Energy Storage System (BESS) Modelling BESSs are becoming an essential component in microgrids management. The technology is becoming more efficient and economically viable than it has been in the past. BESSs provide great flexibility for the supply-demand matching in the short term and present an additional tool for integration of RES. A hybrid BESS model as described by Parisio et al. in [37] will be adopted in this thesis. Due to the hybrid nature of the model, simultaneous charging and discharging are obstructed. The BESS is governed by the following PWA system:

$$x_{\mathrm{b}}(k+1) = \eta_{\mathrm{b1}} x_{\mathrm{b}}(k) + \eta_{\mathrm{b2}} P_{\mathrm{b}}(k)\tau, \tag{2-5}$$

where x_{b} is the current state of charge (SoC) of the battery [kWh], η_{b1} the storage loss efficiency, P_{b} is the power exchanged with the storage [kW], and

$$\eta_{\mathrm{b2}} = \begin{cases} \eta_{\mathrm{ch}}, & \text{if } P_{\mathrm{b}}(k) > 0 \text{ (charging mode)}, \\ \eta_{\mathrm{dch}}, & \text{otherwise (discharging mode)}, \end{cases}$$

where $\eta_{\mathrm{ch}} < 1$ and $\eta_{\mathrm{dch}} = 1/\eta_{\mathrm{ch}}$ are system characteristics accounting for charging and discharging efficiencies. Furthermore, the BESS are subject to the following operating state and input constraints:

$$x_{\mathrm{b}}^{\min} \leq x_{\mathrm{b}}(k) \leq x_{\mathrm{b}}^{\max}, \tag{2-6a}$$

$$P_{\mathrm{b}}^{\min} \leq P_{\mathrm{b}}(k) \leq P_{\mathrm{b}}^{\max}, \tag{2-6b}$$

which limit the minimum and maximum battery SoC and magnitude of power exchange respectively.

Following the standard approach described in [33], a binary variable $\delta_{\mathrm{b}}(k)$ and an auxiliary variable $z_{\mathrm{b}}(k) := \delta_{\mathrm{b}}(k)P_{\mathrm{b}}(k)$ are introduced to transform the system into the following MLD model:

$$x_{\mathrm{b}}(k+1) = \eta_{\mathrm{b1}}x_{\mathrm{b}}(k) - (\eta_{\mathrm{dch}} - \eta_{\mathrm{ch}})z_{\mathrm{b}}(k)\tau + \eta_{\mathrm{dch}}P_{\mathrm{b}}(k)\tau, \tag{2-7a}$$

$$\text{s.t.} \qquad \boldsymbol{E_{b1}}\delta_{\mathrm{b}}(k) + \boldsymbol{E_{b2}}z_{\mathrm{b}}(k)\tau \leq \boldsymbol{E_{b3}}P_{\mathrm{b}}(k)\tau + \boldsymbol{E_{b4}} \tag{2-7b}$$

The system matrices of the BESS system can be found in Appendix A-1.

External Grid Interaction The microgrid under consideration will exclusively operate in grid-connected mode. Thus it is always possible to exchange energy with the external utility grid. The energy exchanges are carried out at the Point of Common Coupling (PCC), where the microgrid is connected to the external utility grid. We assume that different prices are governed for import and export and that these prices are time-varying. Furthermore, it is assumed that at each time instant, the import price is larger than the exporting price. The variable C_{grid} represents the cost or revenue due to interaction with the utility and is given by:

$$C_{\mathrm{grid}}(k) = \max(c_{\mathrm{e,imp}}(k)P_{\mathrm{grid}}(k)\tau, c_{\mathrm{e,exp}}(k)P_{\mathrm{grid}}(k)\tau), \tag{2-8}$$

where C_{grid} is the 'cost' of interaction with the grid [€], $c_{\mathrm{e,imp}}$ and $c_{\mathrm{e,exp}}$ the import and export price of electricity [€/kWh] and $c_{\mathrm{e,imp}} \geq c_{\mathrm{e,exp}}$.

2-2-2 District Heating Network

Aquifer Thermal Energy Storage Modelling ATES is a cost-efficient seasonal storage system that can be used to store large quantities of thermal energy underground [38]. In its purest form, two wells are formed underground as porous formations, also known as aquifers. The system consists of a warm and cold well to store warm and cold water depending on the season. The heat from the stored water in the warm well can be extracted by pumping the water from the warm well to the cold well through a heat exchanger, see Figure 2-2. Similarly, heat can be stored by pumping water from the cold well to the warm well while providing the water with thermal energy from a heat pump.

The authors of [39] propose a control-oriented model of the ATES by describing the system using the stored volume of the water together with the thermal energy content in each well. We have chosen to adopt this model based solely on the dynamics of the thermal energy content of the water stored. Let us define the states of an ATES with the thermal energy of the hot and cold well $S_{\mathrm{h}} \in \mathbb{R}$ and $S_{\mathrm{c}} \in \mathbb{R}$, respectively. The subscript h and c denote the variables belonging to the hot and the cold well, respectively. Now the ATES dynamics are given by:

$$S_{\mathrm{h}}(k+1) = \eta_{\mathrm{h}}(k)S_{\mathrm{h}}(k) - \alpha_{\mathrm{h}}u_{\mathrm{a}}(k)\tau, \tag{2-9a}$$

$$S_{\mathrm{c}}(k+1) = \eta_{\mathrm{c}}(k)S_{\mathrm{c}}(k) + \alpha_{\mathrm{c}}u_{\mathrm{a}}(k)\tau, \tag{2-9b}$$

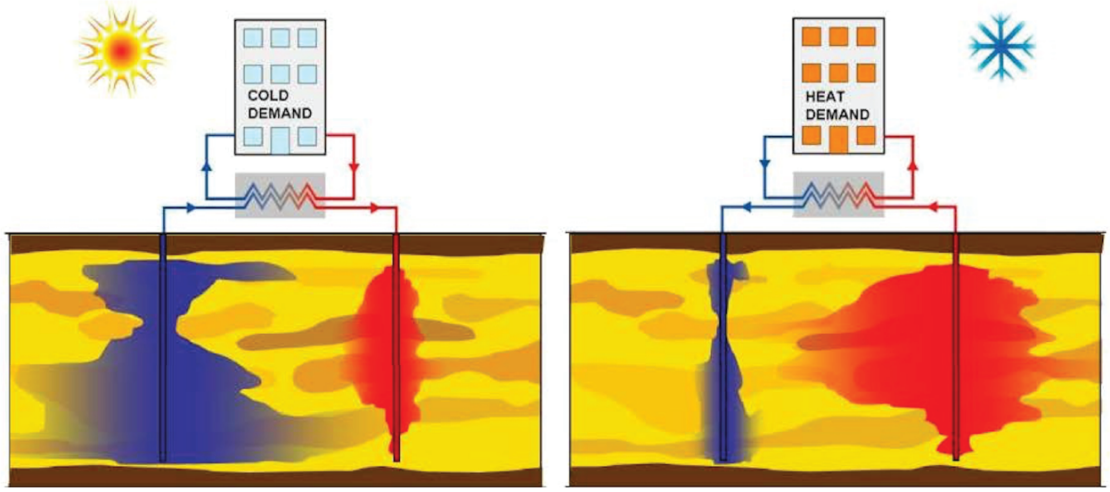

Figure 2-2: Operational modes of an ATES system during warm (left) and cold (right) seasons [39].

where $\eta_{\mathrm{h}}(k) \in (0,1)$ and $\eta_{\mathrm{c}}(k) \in (0,1)$ are the lumped coefficients of thermal energy losses in the aquifers and u_{a} is the control variable corresponding to the pump flow rate of ATES system. The control input u_{a} takes positive values when the heat is withdrawn from the warm well and negative values when the heat is stored in the warm well. Furthermore, $\alpha_{\mathrm{h}}(k) = \rho_{\mathrm{h}} c_{\mathrm{pw}}(T_{\mathrm{h}}(k) - T_{\mathrm{amb}}(k))$, and $\alpha_{\mathrm{c}}(k) = \rho_{\mathrm{h}} c_{\mathrm{pw}}(T_{\mathrm{amb}}(k) - T_{\mathrm{c}}(k))$ are the thermal power coefficients of the warm and cold wells, respectively. Here, the parameters ρ_{h} [kg/m^3], c_{pw} [J/(kgK)] are the density and specific heat capacity of water, respectively. Additionally, $T_{\mathrm{h}}(k)$ [K], $T_{\mathrm{c}}(k)$ [K] and $T_{\mathrm{amb}}(k)$ [K] denote the temperature of the water inside the hot well, cold well and the ambient temperatures, respectively. Moreover, the thermal energy that can be supplied to or taken from the district heating system, Q_{ATES}, can be defined as:

$$Q_{\mathrm{ATES}}(k) = \alpha(k) u_{\mathrm{a}}(k) \tau, \tag{2-10}$$

where $\alpha(k) = \alpha_{\mathrm{h}}(k) + \alpha_{\mathrm{c}}(k)$, is the total power coefficient. The dynamics of the ATES system can be written in the following compact linear-time-varying state-space representation:

$$\boldsymbol{x}_{\mathrm{a}}(k+1) = \boldsymbol{A}_{\mathrm{a}}(k)\boldsymbol{x}_{\mathrm{a}}(k) + \boldsymbol{B}_{\mathrm{a}}(k) u_{\mathrm{a}}(k) \tau, \tag{2-11}$$

where, $\boldsymbol{x}_{\mathrm{a}}(k) = \begin{bmatrix} S_{\mathrm{h}}(k) & S_{\mathrm{c}}(k) \end{bmatrix}^T \in \mathbb{R}^2$ and $u_{\mathrm{a}}(k) \in \mathbb{R}$ are the state vector and input, respectively. Hence the state vectors of the ATES system can be derived to be:

$$\boldsymbol{A}_{\mathrm{a}} = \begin{bmatrix} \eta_{\mathrm{h}} & 0 \\ 0 & \eta_{\mathrm{c}} \end{bmatrix}, \qquad \boldsymbol{B}_{\mathrm{a}} = \begin{bmatrix} -\alpha_{\mathrm{h}} \\ \alpha_{\mathrm{c}} \end{bmatrix}$$

Furthermore, ATES is subject to the following state and input constraints:

$$S_{\mathrm{h}}^{\min} \leq S_{\mathrm{h}}(k) \leq S_{\mathrm{h}}^{\max}, \tag{2-12a}$$

$$S_{\mathrm{c}}^{\min} \leq S_{\mathrm{c}}(k) \leq S_{\mathrm{c}}^{\max}, \tag{2-12b}$$

$$u_{\mathrm{a}}^{\min} \leq u_{\mathrm{a}}(k) \leq u_{\mathrm{a}}^{\max}, \tag{2-12c}$$

where the max and min superscript notation denote the maximum and minimum value of the corresponding variable.

Heat Pump Modelling A heat pump is a device that transfers heat from a low-temperature zone to a higher temperature zone using mechanical work. Generally, a heat pump draws heat from the air, ground or water and uses a vapour compression refrigeration cycle. Recently, heat pumps are gaining more popularity in heating systems due to their high efficiency, characterised by the Coefficient of Performance (COP), which is generally larger than 3 [29]. The output thermal energy of the heat pump delivered at each time step can be calculated by [27]:

$$Q_{\mathrm{hp}}(k) = \mathrm{COP}(k) \cdot P_{\mathrm{hp}}(k)\tau, \tag{2-13}$$

where $Q_{\mathrm{hp}}(k)$ is the output thermal energy of the heat pump [kWh] at time k, P_{hp} is the power to the heat pump [kW] and $\mathrm{COP}(k)$ is the forecasted COP. The COP in the case of the water heat pump used in this thesis is dominated by the difference between the output temperature of the heat pump and the input temperature, which originates from a water source, the Lek river. The following equation is used for calculating the COP (E. Roest van der, personal communication):

$$\mathrm{COP}(k) = 0.0028(T_{\mathrm{out}} + 5 - (T_{\mathrm{in}}(k) - 6)^2) - 0.3276(T_{\mathrm{out}} - T_{\mathrm{in}}(k) + 11) + 13.021, \tag{2-14}$$

where T_{out} is a constant preferred output temperature [K] and $T_{\mathrm{in}}(k)$ is the temperature of the water source [K].

Thermal Energy Balance At each time instant, the thermal energy in the district heating system must be equal or larger than the thermal demand of its users. The following constraint captures the thermal energy balance:

$$Q_{\mathrm{hp}}(k) - Q_{\mathrm{ATES}}(k) - Q_{\mathrm{d}}(k) \geq 0, \tag{2-15}$$

where $Q_{\mathrm{d}}(k)$ is the uncertain variable denoting the thermal energy demand of the system [kWh] at each time instant k. Furthermore, the thermal energy from or to the ATES system depends on the total power coefficient $\alpha(k)$, recall (2-10). We assume that temperature in the wells and the ambient temperature are constant, which means the system is no longer time-varying. Furthermore, it is assumed that we can continue extracting water from the wells when they are fully depleted. This means we are extracting water with ambient temperature. Therefore the total power coefficients depend on the flow direction of the pump and the current thermal energy contents of the well, resulting in:

$$Q_{\mathrm{ATES}}(k) = \begin{cases} \alpha_1(k)u_{\mathrm{a}}(k)\tau, & \text{if } S_{\mathrm{h}}(k) > 0 \,\&\, S_{\mathrm{c}}(k) > 0 \,\&\, u_a(k) > 0, \\ \vdots & \\ \alpha_9(k)u_{\mathrm{a}}(k)\tau, & \text{if } S_{\mathrm{h}}(k) < 0 \,\&\, S_{\mathrm{c}}(k) < 0 \,\&\, u_a(k) < 0, \end{cases} \tag{2-16}$$

Subsequently, (2-11), (2-15) and (2-16) can be transformed into the following MLD system:

$$\boldsymbol{x}_{\mathrm{a}}(k+1) = \boldsymbol{A}_{\mathrm{a}}(k)\boldsymbol{x}_{\mathrm{a}}(k) + \boldsymbol{B}_{\mathrm{a}}(k)u_{\mathrm{a}}(k)\tau, \tag{2-17}$$

$$Q_{\mathrm{hp}}(k) = \boldsymbol{D}_{\mathrm{a}}\boldsymbol{z}_{\mathrm{a}}(k) + Q_{\mathrm{d}}(k), \tag{2-18}$$

$$\boldsymbol{E}_{\mathrm{a1}}\boldsymbol{x}_{\mathrm{a}}(k) + \boldsymbol{E}_{\mathrm{a2}}u_{\mathrm{a}}(k)\tau + \boldsymbol{E}_{\mathrm{a3}}\boldsymbol{z}_{\mathrm{a}}(k) + \boldsymbol{E}_{\mathrm{a4}}\boldsymbol{\delta}_{\mathrm{a}}(k) + \boldsymbol{E}_{\mathrm{a5}}\boldsymbol{b}_{\mathrm{a}}(k) \leq \boldsymbol{E}_{\mathrm{aff}}, \tag{2-19}$$

where $\boldsymbol{z}_{\mathrm{a}} \in \mathbb{R}^3$, $\boldsymbol{\delta}_{\mathrm{a}} \in \mathbb{R}^4$ and $\boldsymbol{b}_{\mathrm{a}} \in \mathbb{R}^3$ denote the vectors of auxiliary, binary and auxiliary binary variables. The full derivation of this system is given in Appendix A-2.

2-2-3 Hydrogen and Water Distribution System

Modelling Hydrogen Trades Similarly to the electricity utility interaction, hydrogen may also be imported or exported. The hydrogen prices are assumed to be constant, and again the importing price is larger than the exporting price.

$$C_{\text{hy}}(k) = \max(c_{\text{hy,imp}} H_{\text{trade}}(k), c_{\text{hy,exp}} H_{\text{trade}}(k)), \tag{2-20}$$

where $C_{\text{hy}}(k)$ is the cost or revenue of trading hydrogen in [€], $c_{\text{hy,imp}}$ and $c_{\text{hy,exp}}$ the import and export price of hydrogen, respectively in [€/kg] and $H_{\text{trade}}(k)$ is the amount of hydrogen traded per time instant k in [kg].

Hydrogen Production and Storage Modelling A water electrolysis system is responsible for providing the hydrogen needed for mobility purposes in the neighbourhood. The produced hydrogen is assumed to be stored directly in a connected reservoir. The amount of hydrogen stored is considered a dynamic state of the system, $x_{\text{el}}(k)$ [kg]. We assume that the energy consumption of the electrolysis system, $P_{\text{el}}(k)$ is a linear function of the produced hydrogen, i.e.

$$H_{\text{el}}(k) = \eta_{\text{hy,el}} P_{\text{el}}(k) \tau, \tag{2-21}$$

The efficiency of the PEM electrolyser $\eta_{\text{hy,el}}$ denotes the amount of power needed per kilogram of hydrogen produced [kW/kg]. The efficiency depends on the maximum power of the electrolyser and the percentage of operation, see Figure 2-3 (E. van der Roest, personal communication). As Figure 2-3 illustrates, the efficiency can be approximated as a PWA function of the current power of the electrolyser, P_{el} and implemented as a lookup table. Furthermore, if surplus energy is absent, hydrogen can be imported from external suppliers as modelled in (2-20). Now the hydrogen storage's dynamics are given by:

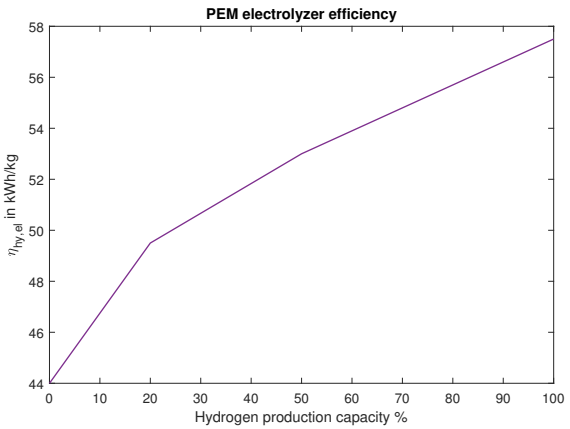

Figure 2-3: Electrolyser efficiency vs. input power.

$$x_{\text{el}}(k+1) = x_{\text{el}}(k) + H_{\text{el}}(k) + H_{\text{trade}}(k) - H_{\text{d}}(k), \tag{2-22}$$

where x_{el} denote the state of the electrolyser's hydrogen buffer, the inputs to the system could be concatenated into $\boldsymbol{u}_{\text{el}}(k) = \begin{bmatrix} H_{\text{el}}(k) & H_{\text{trade}}(k) \end{bmatrix}^T$ and process noise $\omega_{\text{el}}(k) = -H_{\text{d}}(k)$. Note that the hydrogen mass balance is incorporated in the dynamics of the storage model since it acts as a buffer between production and consumption.

Demineralised Water Production and Storage Modelling Demineralised water is used in the system for the production of hydrogen and residential use e.g. dishwashers and washing machines. A high-pressure pump, a membrane module, and a water storage tank form the reverse osmosis system for the production of demineralised water. Generally, water is pressurised and fed into the system where it is separated into a low-salinity product (permeate), and a high-salinity brine (retentate). The demineralised water can now either be used to meet the demineralised water demand or stored in the water tank. The demineralised water

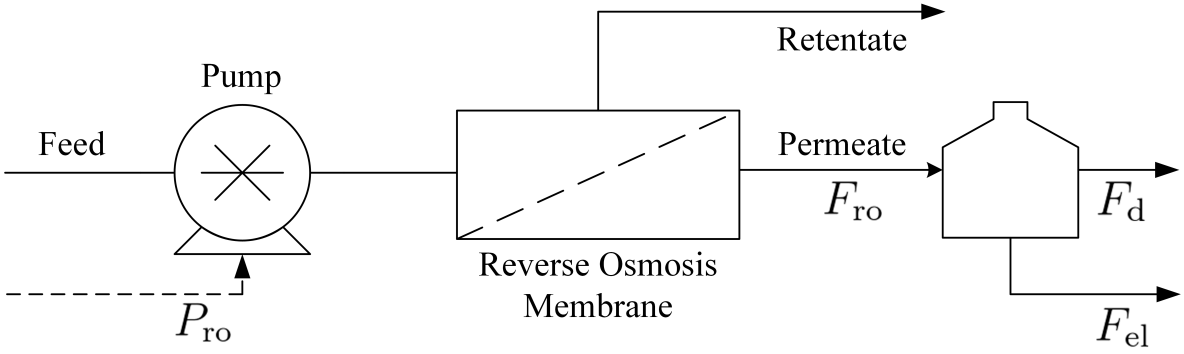

Figure 2-4: Reverse osmosis process for purifying rainwater, water flows depicted as solid arrows and electricity as dashed arrows.

demand is given by, $F_{\mathrm{d}}(k)$, the demineralised water going to the electrolyser by, $F_{\mathrm{el}}(k)$, the produced demineralised water from the reverse osmosis system by, $F_{\mathrm{ro}}(k)$. The demineralised water mass balance is now given by:

$$F_{\mathrm{ro}}(k) - \underbrace{F_{\mathrm{el}}(k)}_{\eta_{\mathrm{dw,hy}} \cdot H_{\mathrm{el}}(k)} - F_{\mathrm{d}}(k) = F_{\mathrm{s}}(k) \tag{2-23}$$

Note that the water storage demand F_{s} can take positive or negative values. Furthermore, note that the electrolyser demand is expressed as the product of an efficiency and electrolyser hydrogen output, i.e. $F_{\mathrm{el}}(k) = \eta_{\mathrm{dw,hy}} \cdot H_{\mathrm{el}}(k)$. Subsequently, the consumed electricity of the reverse osmosis system is expressed as $P_{\mathrm{ro}}(k)\tau = \eta_{\mathrm{el,dw}} \cdot F_{\mathrm{ro}}(k)$ [kW].

Based on the latter equations, the dynamics of the volume in the storage tank, x_{dw}, is given by:

$$x_{\mathrm{dw}}(k+1) = x_{\mathrm{dw}}(k) + F_{\mathrm{ro}}(k) - \eta_{\mathrm{dw,hy}} \cdot H_{\mathrm{el}}(k) - F_{\mathrm{d}}(k), \tag{2-24}$$

where $x_{\mathrm{dw}}(k)$ is the storage volume [m^3].

2-2-4 System Constraints

Energy Balances in the Microgrid Supply and demand matching for all considered energy carriers in the system must be met at every time instant k. For electrical energy this balance is given by the following constraint:

$$P_{\mathrm{b}}(k)\tau = E_{\mathrm{pv}}(k) + \left(P_{\mathrm{grid}}(k) - P_{\mathrm{hp}}(k) - P_{\mathrm{ro}}(k) - P_{\mathrm{el}}(k)\right)\tau, \tag{2-25}$$

where E_{pv} is the aggregate PV generation [kWh]. Now, (2-25) can be substituted in (2-5), and thereby the aggregate input vector of the Power-to-X system can be defined as:

$$\boldsymbol{u}(k) = \begin{bmatrix} P_{\mathrm{grid}}(k)\tau & Q_{\mathrm{hp}}(k) & F_{\mathrm{ro}}(k) & H_{\mathrm{el}}(k) & H_{\mathrm{trade}}(k) & u_{\mathrm{a}}(k) \end{bmatrix}^T \tag{2-26}$$

Operational Constraints The system is subject to storage capacity constraints, decision variable psychical limits, and ramping rate limits. For the BESS and the ATES state constraints and input constraints were given by (2-6) and (2-12), respectively. Similar constraints could be derived for the subsystems for which these constraints were not provided, and could be concatenated into the following constraints:

- **Storage capacity constraints:**

$$\boldsymbol{x}^{\min} \leq \boldsymbol{x}(k) \leq \boldsymbol{x}^{\max}; \tag{2-27}$$

- **Decision variable physical limits:**

$$\boldsymbol{v}^{\min} \leq \boldsymbol{v}(k) \leq \boldsymbol{v}^{\max}; \tag{2-28}$$

- **Ramping rate limits:**

$$\Delta\boldsymbol{v}^{\min} \leq \Delta\boldsymbol{v}(k) \leq \Delta\boldsymbol{v}^{\max}, \tag{2-29}$$

these upper and lower bound values will eventually be presented in Table 4-1 in Section 4-1.

2-2-5 Overall System Model

The individual dynamics of each subsystem can be concatenated in a single compact model, which is suitable for a centralised MPC framework. The resulting overall MLD model is able to capture all dynamics, logic, and constraints of the BESS, ATES, hydrogen storage tank and demineralised water storage tank. One may resort to freely available software HYSDEL [40] for generating the system matrices of the following MLD model:

$$\boldsymbol{x}(k+1) = \boldsymbol{f}(\boldsymbol{x}(k), \boldsymbol{u}(k), \boldsymbol{z}(k), \boldsymbol{\omega}(k)), \tag{2-30a}$$
$$Q_{\mathrm{hp}}(k) = \boldsymbol{D}_{\mathrm{a}}\boldsymbol{z}_{\mathrm{a}}(k) + Q_{\mathrm{d}}(k), \tag{2-30b}$$
$$\boldsymbol{g}(\boldsymbol{x}(k), \boldsymbol{u}(k), \boldsymbol{z}(k)), \boldsymbol{\delta}(k))) \leq \boldsymbol{d}, \tag{2-30c}$$

where,

$$\boldsymbol{f}(\boldsymbol{x}(k), \boldsymbol{u}(k), \boldsymbol{z}(k)), \boldsymbol{\omega}(k)) = \boldsymbol{A}\boldsymbol{x}(k) + \boldsymbol{B_1}\boldsymbol{u}(k) + \boldsymbol{B_2}\boldsymbol{z}(k) + \boldsymbol{B_3}\boldsymbol{\omega}(k), \tag{2-31a}$$

$$\boldsymbol{g}(\boldsymbol{x}(k), \boldsymbol{u}(k), \boldsymbol{z}(k)), \boldsymbol{\delta}(k))) = \boldsymbol{E_1}\boldsymbol{x}(k) + \boldsymbol{E_2}\boldsymbol{u}(k) + \boldsymbol{E_3}\boldsymbol{\delta}(k) + \boldsymbol{E_4}\boldsymbol{z}(k), \tag{2-31b}$$

$$\begin{aligned}
\boldsymbol{x}(k) &= \begin{bmatrix} x_{\mathrm{b}}(k) & \boldsymbol{x}_{\mathrm{a}}{}^{T}(k) & x_{\mathrm{el}}(k) & x_{\mathrm{dw}}(k) \end{bmatrix}^{T}, \\
\boldsymbol{u}(k) &= \begin{bmatrix} P_{\mathrm{grid}}(k) & Q_{\mathrm{hp}}(k) & F_{\mathrm{ro}}(k) & H_{\mathrm{el}}(k) & H_{\mathrm{trade}}(k) & u_{\mathrm{a}}(k) \end{bmatrix}^{T} \\
\boldsymbol{\omega}(k) &= \begin{bmatrix} E_{\mathrm{pv}}(k) & Q_{\mathrm{d}}(k) & T_{\mathrm{in}}(k) & H_{\mathrm{d}}(k) & F_{\mathrm{d}}(k) \end{bmatrix}^{T}, \\
\boldsymbol{\delta}(k) &= \begin{bmatrix} \delta_{\mathrm{b}}(k) & \boldsymbol{\delta}_{\mathrm{a}}^{T}(k) & \boldsymbol{b}_{\mathrm{a}}^{T}(k) \end{bmatrix}^{T}, \\
\boldsymbol{z}(k) &= \begin{bmatrix} z_{\mathrm{b}}(k)\tau & \boldsymbol{z}_{\mathrm{a}}^{T}(k)\tau \end{bmatrix}^{T},
\end{aligned}$$

are the linear dynamical model, states, inputs, disturbances, and MLD variables. Full details on the systems matrices are to be found in Appendix A-3.

2-3 Demand and Generation Forecast

2-3-1 Background

In order to apply MPC strategies for the energy management of a Power-to-X system, the first step is to build forecasting models of the uncertain processes affecting the system. Forecasting state of the art is generally distinguished into two classes, namely, point forecasting and probabilistic forecasting [41–43]. This thesis will further elaborate on point forecasting techniques since it is the most convenient and most applied class of both. In point forecasting, the predicted output at a future time is represented by a single numeric value, which represents the most probable event. Point forecasting methods can be generally classified according to the origin of inputs. Thus, the following two main approaches are considered: models that use endogenous data, i.e. data formed by current and/or lagged time-series input data, and models that make use of exogenous data, which may come from local measurements, e.g. temperature, information from satellite images, Numerical Weather Predictions, and so on [43]. The following point-forecasting methods are considered in the literature:

- **Persistence Models:** These are the simplest models, which are commonly used as a benchmark for more developed models. They assume that conditions (e.g. irradiance, power output, etc.) remain the same between subsequent time steps. An example of a persistence model is 'naive persistence', where the forecasted power will be the same as the last value measured.

- **Time Series Models:** In time series analysis methods are considered which analyse time-series data, where models to predict the future assume that future values are based on previously observed values.

  - Linear stationary models:
    * Auto-Regressive (AR) models
    * Moving-Average (MA) models
    * Auto-Regressive Moving Average (ARMA) models
    * Auto-Regressive eXogenous (ARX) models
    * Auto-Regressive Moving Average with eXogeneous variables (ARMAX) models
  - Linear non-stationary models:
    * Auto-Regressive Integrated Moving Average (ARIMA) models
    * Seasonal ARIMA (SARIMA) models
  - Non-linear stationary models:
    * Non-linear AR-eXogenous (NARMAX) models

- **Artificial Neural Networks:** These are proven to be the most used machine learning techniques in the forecasting of PV generation and load demands. Artificial neural networks do not require the forecaster to model the underlying physical system explicitly. The demand forecast is generated by learning patterns from historical data by mapping the input variables to the output through layers of hidden neurons. Artificial neural networks are highly suitable for discovering non-linear relations between input and output, and the most popular way to train such network is through backpropagation.

- **Support Vector Machines:** These are supervised learning models with associated learning algorithms. Data is analysed and patterns are recognised, which are then used for classification and regression analysis. Support vector machine solutions have proven to be very resistant to overfitting and stand out for their strong generalisation capacity and ability to deal with non-linear problems.

2-3-2 Persistence Forecasting

The uncertain processes that have an effect on the system are contained in disturbance vector $\boldsymbol{\omega}(k)$. This vector includes the solar energy generation E_{pv}, heat demand Q_{d}, heat pump input temperature T_{in}, hydrogen demand H_{d} and demineralised water demand F_{d}. Another exogenous input to be forecast is the electricity price of the utility grid. Figure 2-5 shows these exogenous disturbances on a chosen representative day, i.e. March 3rd. The controller has to make daily decisions about the optimal energy flow in the system; therefore, at most, 24 hours ahead should be forecasted.

Since developing forecasting techniques is not in the scope of research goals, and many exogenous disturbances exist in the system, the choice has been made to use a persistence forecast method, i.e.

$$\bar{\omega}(k) = \omega(k - \frac{\gamma}{\tau}), \tag{2-32}$$

where $\bar{\omega}$ is the point forecast of the exogenous disturbance, k the discrete-time instant, γ the lag in hours and τ is the sampling time in hours. A quick analysis of the autocorrelation

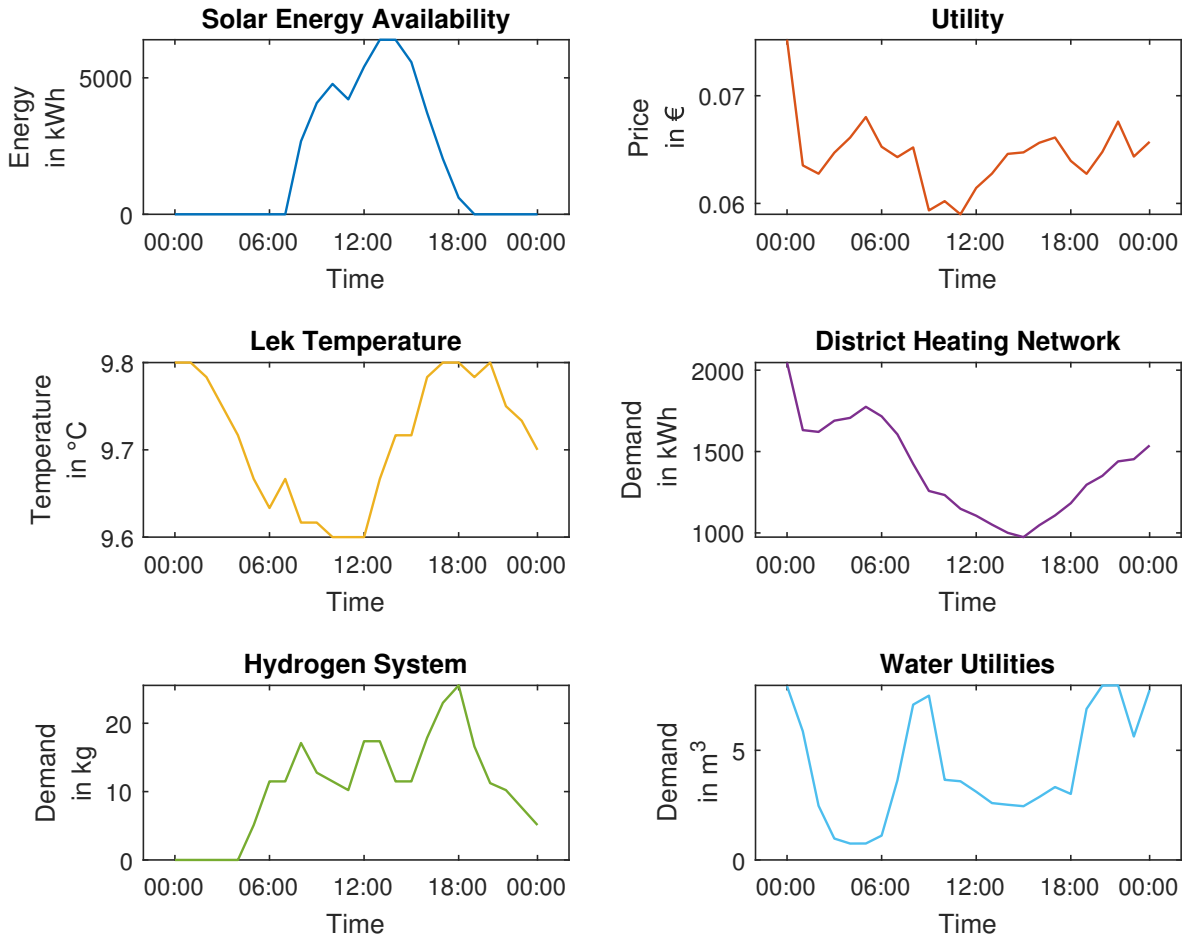

Figure 2-5: Exogenous disturbances on Power-to-X system for the typical day March 3rd.

functions of the historical data time series is required to determine a suitable lag larger than or equal to 24 hours for the persistence method (2-32). Figure 2-6 shows the autocorrelation function of the exogenous disturbances acting on the system. The chosen 'persistence lag' γ for solar power generation, heating demand, water demand, and hydrogen demand is 24 hours. For electricity prices, this value is 28 hours and in the case of water temperature, another persistence model is used, namely using the last measured value of the temperature for the whole forecast horizon.

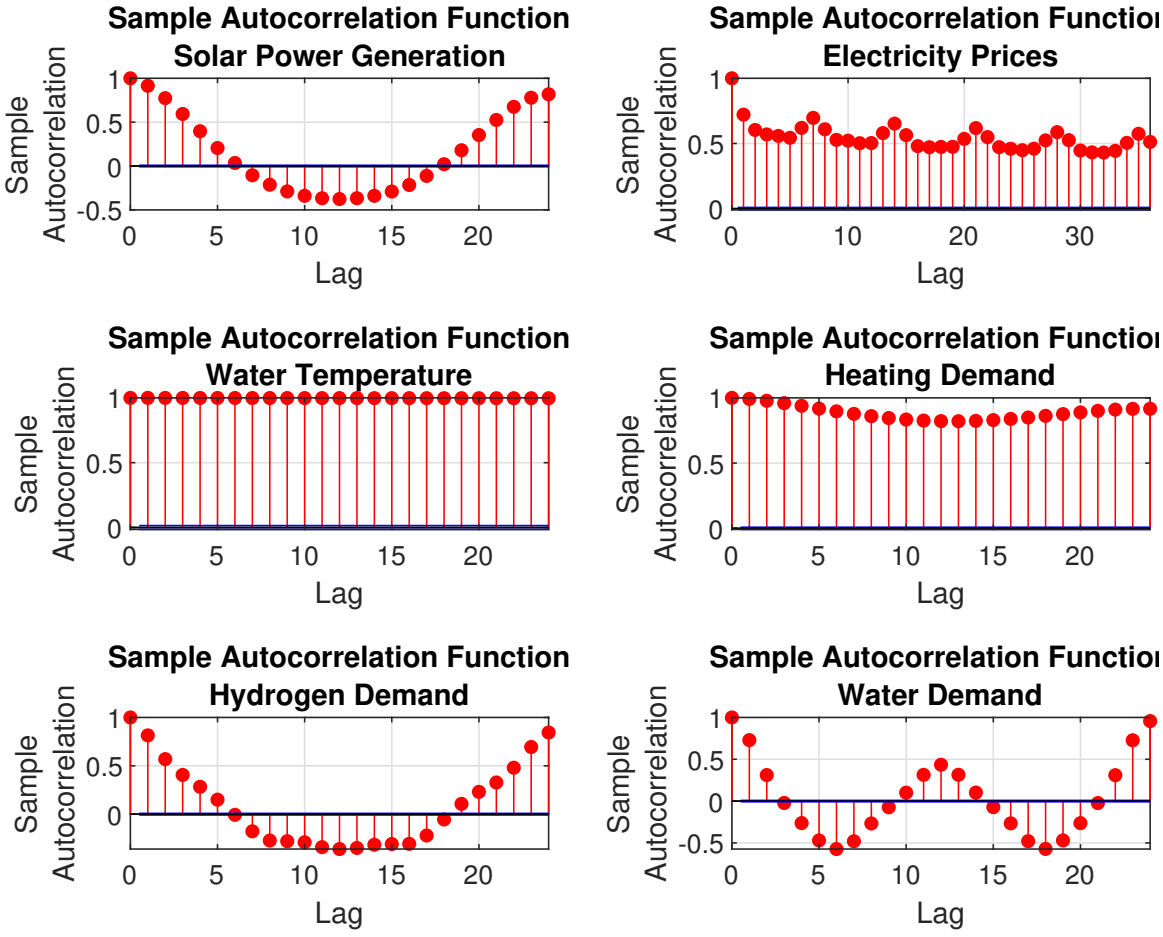

Figure 2-6: Autocorrelation function of exogenous disturbances acting on the system.

Chapter 3

Model Predictive Control for Energy Management of Power-to-X Systems

This chapter presents the main principles and state of the art of the Model Predictive Control (MPC) framework and is structured as follows: First, an introduction of the main principles of MPC is given in Section 3-1; In Section 3-2 an economic MPC formulation is developed for the Power-to-X case study; Then, in Section 3-3 and Section 3-4 a Heuristic Model Predictive Control (HMPC) and Hierarchical Model Predictive Control (HiMPC) schemes are introduced, respectively. Section 3-5 introduces the certainty-equivalent and stochastic frameworks for dealing with uncertainties in the optimal control problem.

3-1 Introduction

In the MPC framework, a finite horizon optimal open-loop control problem is solved online at each sampling time instant, using as an initial condition of the state, the measurement of the state at current time instant [22]. The problem is solved for a fixed range of time in the future, also known as the prediction horizon, see Figure 3-1a. The first control action of the finite control sequence is then applied to the system, after which the control loop is closed. At the next time instant, the described control problem is repeated, and thus MPC is also known at times as Receding Horizon Control. For the employment of MPC, the following information is required [22, 44], as illustrated in Figure 3-1b:

- An objective function expressing which system behaviour and actions are desired;
- A prediction model describing the behaviour of the system subject to actions;
- Constraints on the states, the inputs, and the outputs of the system;
- The possibly known information about future disturbances, e.g. prices or weather forecasts;
- Measurements of the state of the system at the beginning of the current control cycle.

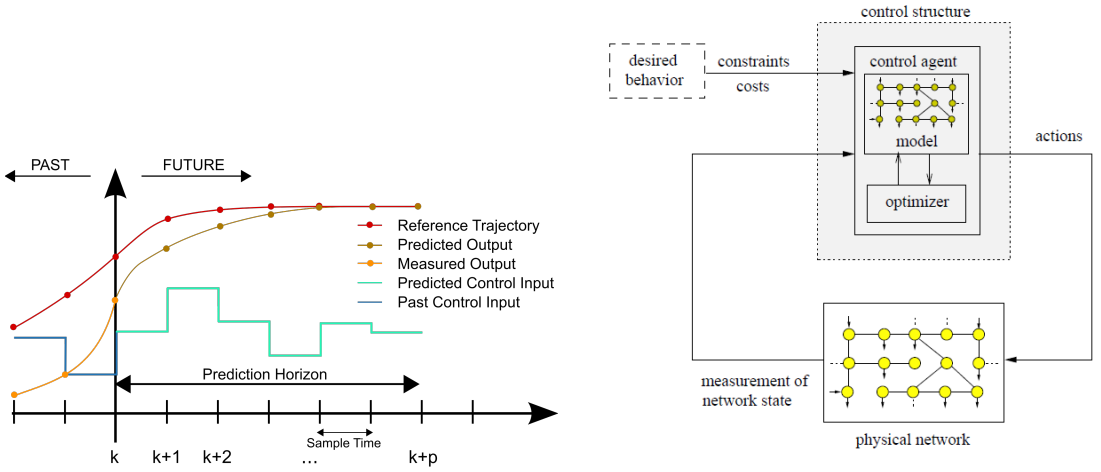

(a) MPC cycle retrieved from https://en.wikipedia.org/wiki/Model_predictive_control.

(b) MPC implementation algorithm [44].

Figure 3-1: MPC main principles and implementation algorithm.

Although MPC has its origins in industrial process applications, due to its advantages over other control structures, many other fields have adapted MPC. Nowadays, MPC is gaining increased attention in areas like power networks, road traffic networks, supply chain management and many more. Some of these advantages which make MPC preferable over ordinary feedback control are [4, 22]:

- MPC can be used to control a great variety of processes, from those with simple dynamics to systems with relatively complex dynamics, e.g. systems with long delay times, non-minimum phase systems or unstable systems;
- The MPC framework can effectively deal with multi-variable processes, compared to conventional control methods;
- The satisfaction of hard input and state constraints for the closed-loop system can be guaranteed, and are easily included in the design phase;
- It is advantageous when future reference values are known;
- Optimisation of some performance criterion is directly incorporated in the controller design;
- It is an open methodology based on certain fundamental principles that allow for future extensions.

Of course, there are also drawbacks to the MPC framework. The greatest drawback is the need for an appropriate model of the process to be available [22]. The design algorithm is based on a-priori knowledge of the system, which can make the controller derivation quite complicated. It is obvious that the benefits obtained will be affected by the discrepancies existing between the real process and the model used. Therefore, the computational complexity may be very demanding, depending on the model complexity [22].

The standard MPC problem solves the described MPC cycle by minimising objective function J_{MPC}. In regulating MPC the goal is to ensure asymptotic stability of the system for the desired sequence of references $\tilde{\boldsymbol{x}}_{\text{ref}}$:

$$\tilde{\boldsymbol{x}}_{\text{ref}}(k) = \begin{bmatrix} x_{\text{ref}}(k|k) & \dots & x_{\text{ref}}(k+N-1|k) \end{bmatrix}^T, \tag{3-1}$$

where N is the prediction horizon of the MPC controller. Furthermore, the system follows a discrete-time dynamic state evolution given by, i.e. (2-2), where for this case, for the sake of ease, a singe-input single-output system is considered and disturbances are not included. The control sequence computed as a result of the optimisation is contained in vector $\tilde{\boldsymbol{u}}$, i.e.:

$$\tilde{\boldsymbol{u}}(k) = \begin{bmatrix} u(k|k) & \dots & u(k+N-1|k) \end{bmatrix}^T, \tag{3-2}$$

The general MPC optimal control problem is defined as follows:

$$\min_{\tilde{\boldsymbol{u}}(k)} \quad J_{\text{MPC}}(x(k), \tilde{\boldsymbol{x}}_{\text{ref}}(k), \tilde{\boldsymbol{u}}(k)) \tag{3-3}$$

$$\text{s.t.} \quad x(k+i|k) = f(x(k), \tilde{\boldsymbol{u}}(k)), \qquad \forall i \in \mathbb{Z}_{[0,N-1]}, \tag{3-4a}$$

$$u(k+i|k) \in \mathbb{U}, \;\; x(k+i|k) \in \mathbb{X}, \qquad \forall i \in \mathbb{Z}_{[0,N-1]}, \tag{3-4b}$$

$$x(k+N|k) \in \mathbb{X}_f, \tag{3-4c}$$

where,

$$J_{\text{MPC}}(x(k), \tilde{\boldsymbol{x}}_{\text{ref}}(k), \tilde{\boldsymbol{u}}(k)) = \sum_{i=0}^{N-1} \left(l(x(k), x_{\text{ref}}(k+i|k), u(k+i|k)) \right) \tag{3-5}$$

$$+ V_f(x(k+N|k), x_{\text{ref}}(k+N-1|k)), \tag{3-6}$$

where the objective function J_{MPC} consists of stage cost function l and terminal cost function $V_f(x(k+N|k))$, where the latter only depends on the terminal state which is contained in the terminal set, i.e. $x(k+N|k) \in \mathbb{X}_f$. Time increment i exists in the set of integer numbers in the interval $[0, N-1]$, i.e. $i \in \mathbb{Z}_{[0,N-1]}$ and the control input and state are constrained by sets $\mathbb{U}$ and $\mathbb{X}$, respectively. The first entry of the vector $\tilde{\boldsymbol{u}}$ is the only control input applied to the system in this time instant. After that, new state measurements will be available. Then the optimisation is repeated using the updated state measurement.

3-2 Optimal Control Problem Formulation for Energy Management

The Energy Management System (EMS) of a Power-to-X system has the purpose of making decisions about the system's energy flows while taking into account uncertainties, control objectives (Section 3-2-1) and system constraints (Section 3-2-2). The interaction of the EMS with the Power-to-X system is visualised in Figure 3-2. The ordinary EMS tasks are to determine the energy flows of storage, generation and production units within the system on an hourly base. However, for Power-to-X, the main control challenge arose from the fact there is a temporal mismatch between electrical energy production and thermal energy demand, as shown in Figure 1-4. The Aquifer Thermal Energy Storage (ATES) system is suitable to solve this mismatch since it allows for thermal energy storage for multiple months. However, this leaves us with multiple timescales, the 'slow' ATES system and the hourly tasks of the EMS for the rest of the Power-to-X system. Thus another task for the EMS is to schedule long-term heat storage planning. In the remainder of this section, MPC as EMS for Power-to-X systems will be elaborated on.

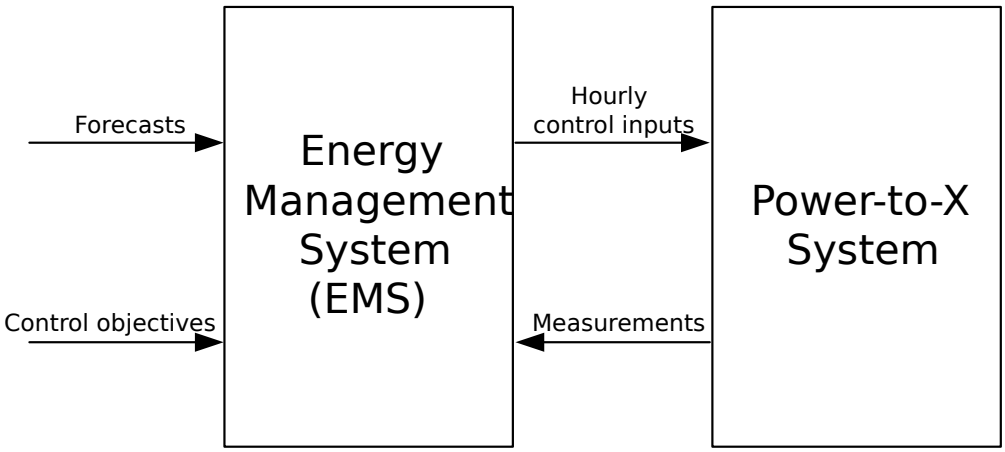

Figure 3-2: Interaction of the EMS with the Power-to-X system.

3-2-1 Objective Function

MPC optimal control formulations where a certain desired objective is directly incorporated in the objective function is called Economic MPC [4, 45]. The Economic MPC objective functions suitable for any optimal control problem concerning optimal energy flows within an energy system are concerned with minimising operational expenses, environmental concerns, maintaining generator and storage life-cycles, and seasonal energy plan tracking. Any combination of these objective functions may be considered, which may eventually result in multi-objective optimisation.

Bill Minimisation: This objective is concerned with minimising the operational expenses of the system. Generally, it consists of revenues and costs due to importing or exporting of energy vectors, generator costs, and converter costs. In this thesis, we neglect the costs of generators and converters. Consequently, an objective function suitable for bill minimisation is described by the following equation [37, 46]:

$$l_{\text{bill}}(k) = C_{\text{grid}}(k) + C_{\text{hy}}(k), \tag{3-7}$$

where C_{grid} and C_{hy} are the costs of external grid interaction of electricity and hydrogen [€], respectively. The external grid interaction costs and hydrogen trading costs were given by (2-8) and (2-20), respectively

Carbon Dioxide Emission Reduction: This objective function is an environmental one and is concerned with minimising the carbon dioxide emissions originating from the Power-to-X system. The system may be responsible for carbon dioxide emissions by importing energy from non-renewable energy sources or can contribute to saving carbon dioxide emissions by producing hydrogen for zero-emission hydrogen vehicles. The environmental stage cost function is:

$$l_{\text{env}}(k) = \max(s_{\text{el}} P_{\text{grid}}(k)\tau, 0) - s_{\text{hy}} H_{\text{el}}(k), \tag{3-8}$$

where P_{grid} is the power imported or exported from the utility grid [kW], s_{el} the estimated carbon dioxide contribution per energy imported from the grid [kg/kWh], $H_{\text{el}}(k)$ the produced hydrogen in the system and s_{hy} the estimated saved carbon dioxide emissions from driving a hydrogen-fueled vehicle as contrary to a conventional vehicle.

Maintaining Asset Life Time: Electrolysers, heat pumps and battery energy storage systems (BESSs) are subject to life-time deterioration due to switching of modes, i.e. on/off, charging/discharging. An objective function minimising these phenomena is given by [46]:

$$l_{\text{life}}(k) = 0.5 \cdot |\Delta\text{sgn}(P_{\text{b}}(k))| + |\Delta\text{sgn}(P_{\text{hp}}(k))| + |\Delta\text{sgn}(P_{\text{el}}(k))| + |\Delta\text{sgn}(P_{\text{ro}}(k))|, \tag{3-9}$$

where P_{b} is the power to or extracted from the battery [kW], P_{hp} the power to the heat pump [kW], P_{el} the power input of the electrolyser [kW] and P_{ro} is the power to the reverse osmosis system [kW]. Note that the term with P_{b} is multiplied by a factor of 0.5 since it is the only power input that can take negative and positive values.

Energy Plan Tracking: In EMS of microgrids, it is common to implement pre-scheduled targets for manipulated inputs and/or states in the MPC objective [47–49]. These targets may follow from pre-schedulers acting on slower time-rates, i.e. day ahead vs hourly, or from day-ahead market agreements. The pre-scheduler problem is either formulated as a common optimisation problem or in some cases, implemented as an MPC controller. The goal attained by the objective is to penalise the deviation from the schedule by assigning a cost to the difference, i.e.:

$$l_{\text{sched}}(k) = \|(\boldsymbol{v}_{\text{sched}}(k) - \boldsymbol{v}(k)\|_2 + \|(\boldsymbol{x}_{\text{sched}}(k) - \boldsymbol{x}(k)\|_2, \tag{3-10}$$

where $\boldsymbol{v}_{\text{sched}}$ is a vector containing the optimal operation limits and $\boldsymbol{x}_{\text{sched}}$ the optimal states passed by the pre-scheduler. By introducing such terms in the objective, the MPC controller aims to minimise deviations by changing settings of the storage devices.

Multi-Objective Optimisation: For this case study, an economic objective function is chosen, i.e. (3-7). Furthermore, in the HiMPC framework, some reference has to be tracked, i.e. (3-10) which will result in a multi-objective optimisation problem. The environmental objective of carbon dioxide reduction is not explicitly taken into account since the Power-to-X system is already highly optimised for environmental design objectives.

The dynamical model of the Power-to-X system is a hybrid one. Therefore a Mixed-Integer Optimisation has to be solved. In the case of a quadratic norm minimisation (3-10), this problem is a Mixed Integer Quadratic Programming (MIQP) problem which is generally harder to solve than a Mixed Integer Linear Programming (MILP) problem. Therefore the tracking objective is reformulated using the first norm, i.e.

$$l_{\text{sched}}(k) = \|(\boldsymbol{v}_{\text{sched}}(k) - \boldsymbol{v}(k)\|_1 + \|(\boldsymbol{x}_{\text{sched}}(k) - \boldsymbol{x}(k)\|_1, \tag{3-11}$$

When the earlier introduced economic MPC objective functions, (3-7) and (3-11) are combined, the optimisation problem results in a multi-objective optimisation problem, with the following cost:

$$J_{\text{EMPC}} = \sum_{k=0}^{N-1} (l_{\text{bill}}(k) + w_{\text{sched}} l_{\text{sched}}(k)), \tag{3-12}$$

where w_{sched} are the costs/weights assigned to the deviation of the schedule. These weights can be tuned to assign importance to the corresponding goal.

3-2-2 Optimisation Constraints and Feasibility

The MPC formulation of the EMS problem of Power-to-X systems is subject to constraints, composed of the Mixed Logical Dynamical (MLD) model's constraints, energy balance constraints, operational constraints and input/state constraints. In Section 2-2-5, the system's dynamics were compactly written in an MLD formulation (2-30a). The operational constraints are combined into (2-30c). Due to the ability of some energy carriers to be imported/exported from an external party, the problem would not quickly become infeasible in the sense that the grid can account for any unaccounted imbalances of the energy carriers. In the case that the problem becomes infeasible, the storage limit constraints could be recast into soft constraints with the introduction of slack variables [22], i.e.:

$$\boldsymbol{x}^{\min} - \boldsymbol{\rho}(k) \leq \boldsymbol{x}(k) \leq \boldsymbol{x}^{\max} + \boldsymbol{\rho}(k), \tag{3-13}$$

$$0 \leq \boldsymbol{\rho}(k) \leq \boldsymbol{\rho}^{\max}, \tag{3-14}$$

and,

$$l_{\text{slack}}(k) = \|\text{diag}(\boldsymbol{w}_{\boldsymbol{\rho}})\boldsymbol{\rho}(k)\|_1, \tag{3-15}$$

where (3-13) and (3-14) are the newly introduced constraints and (3-15) is the objective function for slack variable minimisation and $\boldsymbol{\rho}$ the vector containing the slack variables. The weight vector $\boldsymbol{w}_{\boldsymbol{\rho}}$ is tuned accordingly to allow some constraint violations of the corresponding storage element.

3-3 Heuristic MPC

3-3-1 Introduction

The HMPC controller is the first approach to solving a Power-to-X optimal control problem for energy management purposes as highlighted before. The proposed scheme will solve this problem within a single control layer, as opposed to HiMPC which consists of multiple interacting control layers. The proposed HMPC will act as the EMS of the Power-to-X system. Therefore, the decision variables computed by the HMPC scheme will be provided to the system as hourly set-points for local regulating controllers. The HMPC sampling time $\tau^{\mathrm{h}} = 1\,\mathrm{hour}$ with a prediction horizon of $N^{\mathrm{h}} = 24$ hours. Though, this horizon is too short of anticipating for seasonal differences and making use of the long-term ATES system. Therefore the proposed HMPC controller will provide a solution to the short horizon by including a terminal cost on the thermal energy content of the ATES hot well.

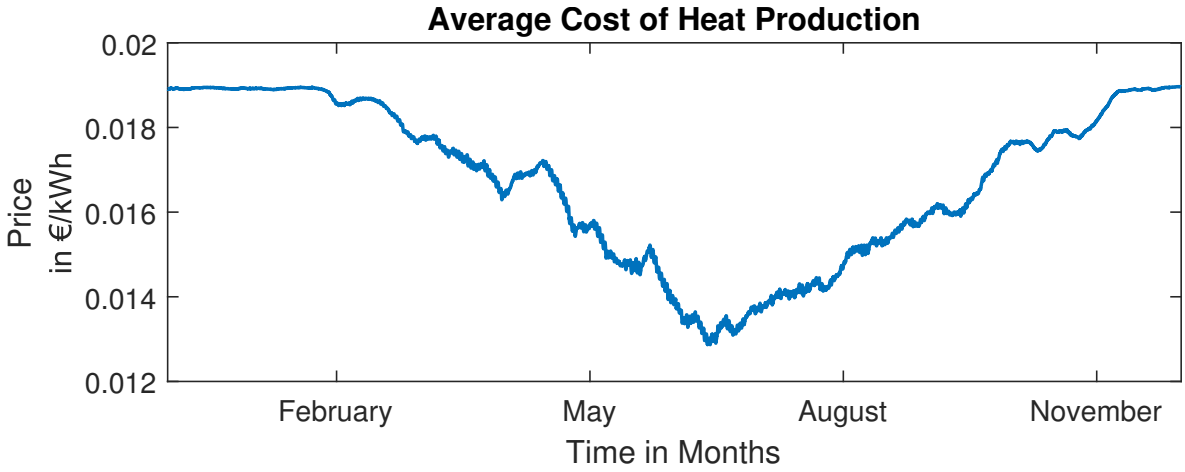

Figure 3-3: Average heat production prices for the year 2013.

Figure 3-3 shows the average heat production prices C_{heat} for a representative year. Obvious is that in the warmer months, the price per kWh of heat is much lower than in the colder winter months. The value of C_{heat} can also be viewed as the value of heat at a certain time. Therefore, a terminal cost incorporating the phenomenon that producing heat in the summer is more beneficial than in the winter is given by:

$$V_f^{\mathrm{h}} = \Delta C_{\mathrm{heat}}(k^{\mathrm{h}} + N^{\mathrm{h}}|k^{\mathrm{h}}) \cdot (\eta_{\mathrm{a}})^{\kappa} \cdot S_{\mathrm{h}}(k^{\mathrm{h}} + N^{\mathrm{h}}|k^{\mathrm{h}}), \tag{3-16}$$

where $\Delta C_{\mathrm{heat}}(k^{\mathrm{h}} + N^{\mathrm{h}}|k^{\mathrm{h}}) = C_{\mathrm{heat}}(k^{\mathrm{h}} + N^{\mathrm{h}}|k^{\mathrm{h}}) - C_{\mathrm{heat}}(k^{\mathrm{h}} + N^{\mathrm{h}} + 720 \cdot \kappa|k^{\mathrm{h}})$ is the difference value of produced heat of present-day versus κ months ahead, η_{a} is the storage efficiency of heat for the ATES system, and $S_{\mathrm{h}}(k^{\mathrm{h}} + N^{\mathrm{h}}|k^{\mathrm{h}})$ is the terminal state of the ATES warm well. Furthermore, if ΔC_{heat} is smaller than zero, it would mean that heat storage is minimised, which is never desirable. Therefore some rules have to be included. Furthermore, note that it was assumed that a month contains 720 hours.

The HMPC controller has three tuning variables, namely, the horizon κ determining how many months in the future the heat energy is estimated to be used, threshold ψ roughly determines in which month heat should be started to be produced and λ the variable preventing greedy use of the heat storage in months where heat is used. These rules are summarised in Algorithm 1.

Algorithm 1: Heuristics in single-layer MPC

Calculate difference of heat energy value i.e.
$\Delta C_{\text{heat}}(k^{\text{h}} + N^{\text{h}}|k^{\text{h}}) = C_{\text{heat}}(k^{\text{h}} + N^{\text{h}}|k^{\text{h}}) - C_{\text{heat}}(k^{\text{h}} + N^{\text{h}} + 720 \cdot \kappa|k^{\text{h}})$
if $\Delta C_{\text{heat}}(k^{\text{h}} + N^{\text{h}}|k^{\text{h}}) > \psi$ **then**
  $\Delta C_{\text{heat}}(k^{\text{h}} + N^{\text{h}}|k^{\text{h}}) = C_{\text{heat}}(k^{\text{h}} + N^{\text{h}}|k^{\text{h}}) - C_{\text{heat}}(k^{\text{h}} + N^{\text{h}} + 720 \cdot \kappa|k^{\text{h}})$
else
  $\Delta C_{\text{heat}}(k^{\text{h}} + N^{\text{h}}|k^{\text{h}}) = \lambda$
end

3-3-2 Problem Formulation

The HMPC optimisation problem is given by the following equations:

$$\min_{\tilde{\boldsymbol{v}}^{\text{h}}(k^{\text{h}}),\tilde{\boldsymbol{\rho}}^{\text{h}}(k^{\text{h}})} \quad \sum_{i=0}^{N^{\text{h}}-1} \Big(C^{\text{h}}_{\text{grid}}(k^{\text{h}}+i|k^{\text{h}}) + C^{\text{h}}_{\text{hy}}(k^{\text{h}}+i|k^{\text{h}}) + w^{\text{h}}_{\text{slack}} \cdot \|\text{diag}(\boldsymbol{w}^{\text{h}}_{\boldsymbol{\rho}})\boldsymbol{\rho}^{\text{h}}(k^{\text{h}}+1+i|k^{\text{h}})\|_1 \Big)$$
$$+ \Delta C_{\text{heat}}(k^{\text{h}} + N^{\text{h}}|k^{\text{h}}) \cdot (\eta_{\text{a}})^{\kappa} \cdot S_{\text{h}}(k^{\text{h}} + N^{\text{h}}|k^{\text{h}}) \tag{3-17}$$

s.t. MLD system dynamics (2-30), (3-18a)

$$\boldsymbol{x}^{\min} - \boldsymbol{\rho}^{\text{h}}(k^{\text{h}}+i|k^{\text{h}}) \leq \boldsymbol{x}(k^{\text{h}}+i|k^{\text{h}}) \leq \boldsymbol{x}^{\max} + \boldsymbol{\rho}^{\text{h}}(k^{\text{h}}+i|k^{\text{h}}), \tag{3-18b}$$

$$\boldsymbol{v}^{\min} \leq \boldsymbol{v}^{\text{h}}(k^{\text{h}}+i|k^{\text{h}}) \leq \boldsymbol{v}^{\max}, \tag{3-18c}$$

$$0 \leq \boldsymbol{\rho}^{\text{h}}(k^{\text{h}}+i|k^{\text{h}}) \leq \boldsymbol{\rho}^{\max}, \tag{3-18d}$$

$$\forall i \in \mathbb{Z}_{[0,N^{\text{h}}-1]},$$

where (3-17) is the objective function, including slack variable ($\boldsymbol{\rho}^{\text{h}} \in \mathbb{R}^5$) minimisation, (3-18a) - (3-18d) are the system constraints containing the MLD system model and state, input and slack variable constraints. The HMPC decision vector is given by:

$$\boldsymbol{v}^{\text{h}} = \begin{bmatrix} \boldsymbol{u}^T(k) & \boldsymbol{\delta}^T(k) & \boldsymbol{z}^T(k) \end{bmatrix}^T, \tag{3-19}$$

where the input vector, binary input vector and vector of auxiliary variables were introduced in Section 2-2-5.

3-3-3 Tuning

For the use of the latter introduced HMPC scheme, three parameters have to be tuned. First of all, we have found that κ, the horizon of ΔC_{heat} is best suitable as $\kappa = 6$. This can be chosen beforehand because it is likely that heat energy is going to be utilised six months in advance in a Power-to-X system. Illustrative comparison of tunable parameters is shown in Figure 3-4. The threshold ψ determines when the controller should start accounting for storing heat. The figure below compares three cases of ψ for constant κ and λ. As expected, smaller values of ψ cause the controller to act in earlier months in terms of storing heat.

On the other hand, the parameter λ accounts for the 'greediness' of using heat energy in months that heat is not stored. This is again illustrated in the figure below, now for varying λ and constant κ and ψ. What we observe is that in the case of the smallest value of $\lambda = 40$, the stored heat is depleted as quick as March, which is not desirable. Subsequently, too large values of λ result in too little stored heat withdrawal, e.g. for $\lambda = 60$.

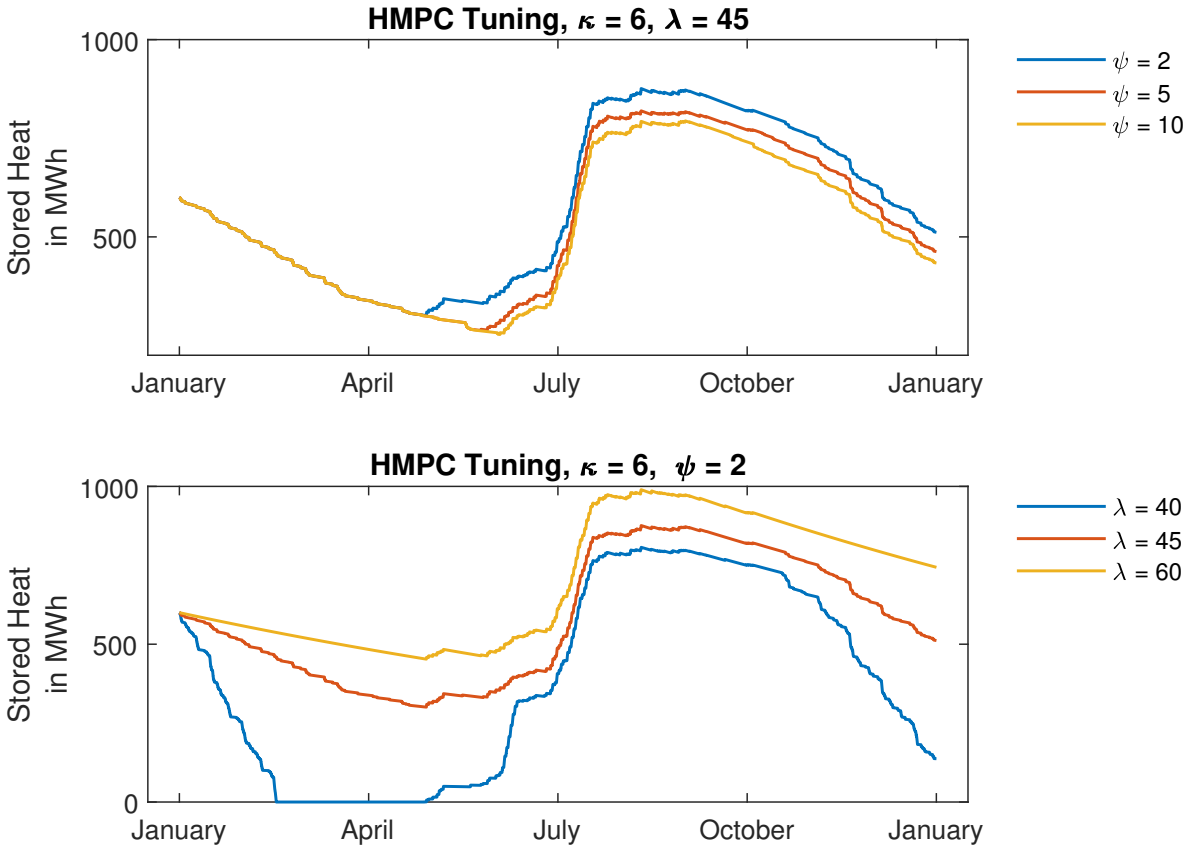

Figure 3-4: Tuning of the HMPC control scheme, upper plot varies ϕ and the lower plot varies λ while keeping other parameters constant.

3-4 Hierarchical MPC

3-4-1 Introduction

In the previous section, a heuristic approach was presented for MPC of the Power-to-X system. Though, the most straightforward way to deal with multiple timescales in the plant or disturbance processes is time-scale decomposition [24, 50]. Time-scale decomposed systems are controlled by a cascade of MPC controllers, each assigned to a layer in the hierarchy. Consequently, control schemes of this form are often referred to as multi-layer control schemes or hierarchical control schemes. The higher layer in the hierarchy generally computes state and/or manipulated variable set-points for the layer below. An example of such a time-scale decomposed control scheme is visualised in Figure 3-5. In this case, we see that the control scheme is decomposed into three timescales, where intermediate layer communication is present, i.e. passing of set-points and state measurements. Information from interlayer objectives can be utilised at adjacent lower layers as setpoints to be tracked. This can be achieved by conventional setpoint tracking in the objective function, introducing terminal states to be reached or average tracking. This is visualised in Figure 3-5 with arrows interconnecting the interlayer connections.

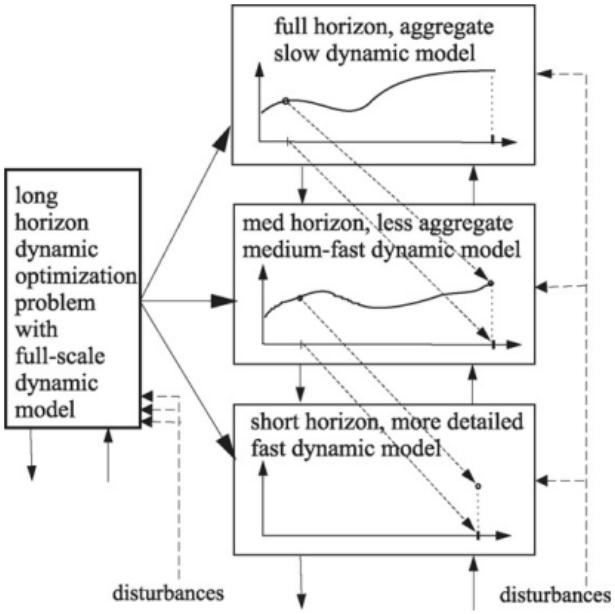

Figure 3-5: Example of a time-scale decomposition into three layers [50].

Even though time-scale decomposition may seem like an intuitive solution for dealing with multi-timescale systems, it is not straightforward to come up with models for each control layer. What is very often seen in the literature is time-scale decomposition models based on singular perturbation theory, which provides a natural framework for modelling, analysing and controlling these multiple time-scale processes [24]. Other methods for coming up with models for separate layers may be by resampling an existing model [51], by assuming static models [44, 51], i.e. assuming that the reference passed to a lower level is reached in the higher-level time interval, or by approximating the lower level's closed-loop system [52].

3-4-2 Problem Formulation

A HiMPC control scheme suitable for the current case-study suffices with two layers, where the upper-layer should encapsulate seasonal differences, and the lower-layer interacts with the Power-to-X system. This scheme results in one as depicted in Figure 3-6. The lower-layer problem acts on an hourly base with a daily prediction horizon, whereas the upper-layer has a sampling time of $\tau^{\mathrm{u}} = 720\,\mathrm{hours}$ and a prediction horizon of a year, i.e. $N^{\mathrm{u}} = 12\,\mathrm{months}$. The lower-layer MPC (LL-MPC) acts as the EMS of the Power-to-X system, whereas the upper-layer MPC (UL-MPC) scheme acts as a supervisory control layer providing ATES hot well references for the lower-layer.

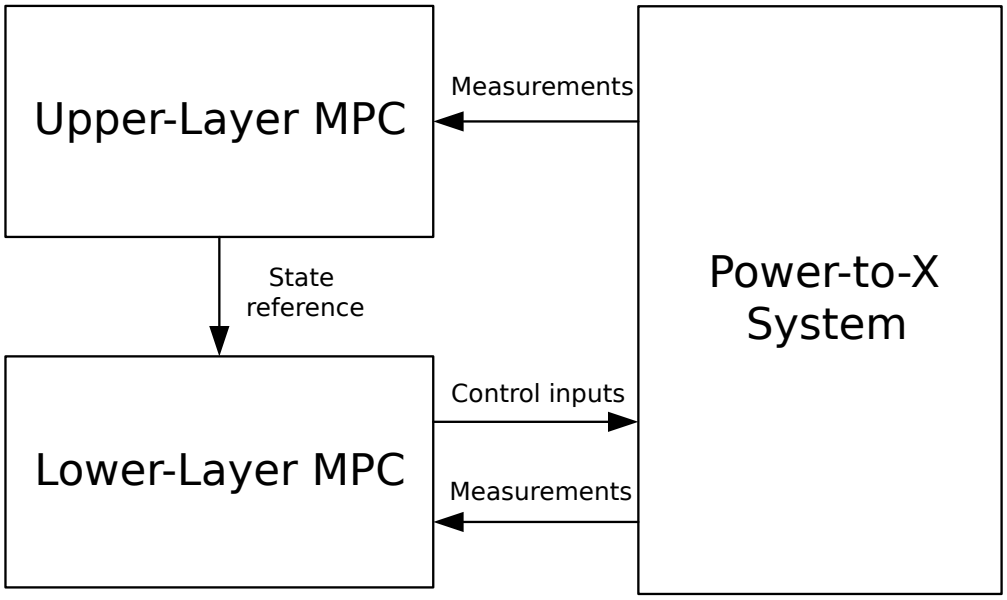

Figure 3-6: Proposed HiMPC scheme. Consists of two interacting layers, the UL-MPC providing ATES hot well reference values for the LL-MPC which acts as EMS

Upper-Layer Problem The UL-MPC is concerned with providing monthly set-points of the heat storage for the LL-MPC to track. Therefore the upper-layer is an anticipatory controller taking into account seasonal differences of the solar power availability and thermal energy demands. The prediction model of the upper-layer problem only consists of the ATES system dynamics, resampled at sampling time τ^{u}. Since the dynamics of the other storage elements are not taken into account of the optimisation problem, the electrical energy balance, hydrogen mass balance and demineralised volume balance have to be implemented as constraints explicitly. These balances must be fulfilled in an aggregated manner for one month, i.e. by scaling with τ^{u}

The upper-layer optimisation problem is given by:

$$\min_{\tilde{\boldsymbol{v}}^{\mathrm{u}}(k^{\mathrm{u}}),\tilde{\boldsymbol{\rho}}^{\mathrm{u}}(k^{\mathrm{u}})} \quad \sum_{i=0}^{N^{\mathrm{u}}-1} (C^{\mathrm{u}}_{\mathrm{grid}}(k^{\mathrm{u}}+i|k^{\mathrm{u}}) + C^{\mathrm{u}}_{\mathrm{hy}}(k^{\mathrm{u}}+i|k^{\mathrm{u}}) + w^{\mathrm{u}}_{\mathrm{slack}} \cdot \|\mathrm{diag}(\boldsymbol{w}^{\mathrm{u}}_{\boldsymbol{\rho}}) \cdot \boldsymbol{\rho}^{\mathrm{u}}(k^{\mathrm{u}}+1+i|k^{\mathrm{u}})\|_1) \tag{3-20}$$

s.t. District Heating System (2-17), (2-18) and (2-19), (3-21a)

$$\boldsymbol{x}^{\min}_{\mathrm{a}} - \boldsymbol{\rho}^{\mathrm{u}}(k^{\mathrm{u}}+1+i|k^{\mathrm{u}}) \leq \boldsymbol{x}_{\mathrm{a}}(k^{\mathrm{u}}+1+i|k^{\mathrm{u}}) \leq \boldsymbol{x}^{\max}_{\mathrm{a}} + \boldsymbol{\rho}^{\mathrm{u}}(k^{\mathrm{u}}+1+i|k^{\mathrm{u}}), \tag{3-21b}$$

$$\boldsymbol{v}^{\min}\tau^{\mathrm{u}} \leq \boldsymbol{v}(k^{\mathrm{u}}+i|k^{\mathrm{u}}) \leq \boldsymbol{v}^{\max}\tau^{\mathrm{u}}, \tag{3-21c}$$

$$0 \leq \boldsymbol{\rho}^{\mathrm{u}}(k^{\mathrm{u}}+1+i|k^{\mathrm{u}}) \leq \boldsymbol{\rho}^{\max}, \tag{3-21d}$$

$$E_{\mathrm{pv}}(k^{\mathrm{u}}+i|k^{\mathrm{u}}) - (P_{\mathrm{grid}}(k^{\mathrm{u}}+i|k^{\mathrm{u}}) - \frac{Q_{\mathrm{hp}}(k^{\mathrm{u}}+i|k^{\mathrm{u}})}{\mathrm{COP}(k^{\mathrm{u}}+i|k^{\mathrm{u}})} - \eta_{\mathrm{el,dw}} \cdot F_{\mathrm{ro}}(k^{\mathrm{u}}+i|k^{\mathrm{u}}) - \frac{1}{\eta_{\mathrm{hy,el}}} \cdot H_{\mathrm{el}}(k^{\mathrm{u}}+i|k^{\mathrm{u}}))\tau^{\mathrm{u}} \geq 0, \tag{3-21e}$$

$$H_{\mathrm{el}}(k^{\mathrm{u}}+i|k^{\mathrm{u}}) + H_{\mathrm{trade}}(k^{\mathrm{u}}+i|k^{\mathrm{u}}) - H_{\mathrm{d}}(k^{\mathrm{u}}+i|k^{\mathrm{u}}) \geq 0, \tag{3-21f}$$

$$F_{\mathrm{ro}}(k^{\mathrm{u}}+i|k^{\mathrm{u}}) - \eta_{\mathrm{dw,hy}} H_{\mathrm{el}}(k^{\mathrm{u}}+i|k^{\mathrm{u}}) - F_{\mathrm{d}}(k^{\mathrm{u}}+i|k^{\mathrm{u}}) \geq 0, \tag{3-21g}$$

$$\forall i \in \mathbb{Z}_{[0,N-1]},$$

where (3-20) is the objective function to be minimised, (3-21a) is the heat system's MLD system for a monthly sampling time, (3-21b)-(3-21d) are the state, input and slack variable bounds. The monthly energy balance is captured in (3-21e), the hydrogen mass balance by (3-21f) and the demineralised water balance is given by (3-21g). The vector containing the slack variables is defined as $\boldsymbol{\rho}^{\mathrm{u}} \in \mathbb{R}^2$ for transforming the state $\boldsymbol{x}_{\mathrm{a}} \in \mathbb{R}^2$ limit constraints into soft constraints. Decision vector $\boldsymbol{v}^{\mathrm{u}}$ looks similar to the HMPC controller's decision vector (3-19) with the exception of all decision variables related to the battery storage.

Lower-Layer Problem The LL-MPC is concerned with the same tasks as described for the EMS of Power-to-X systems, while now also tracking monthly set-points from the upper-layer optimisation. The lower-layer problem is given by:

$$\min_{\tilde{\boldsymbol{v}}^{\mathrm{l}}(k^{\mathrm{l}}),\tilde{\boldsymbol{\rho}}^{\mathrm{l}}(k^{\mathrm{l}})} \quad \sum_{i=0}^{N^{\mathrm{l}}-1} (C^{\mathrm{l}}_{\mathrm{grid}}(k^{\mathrm{l}}+i|k^{\mathrm{l}}) + C^{\mathrm{l}}_{\mathrm{hy}}(k^{\mathrm{l}}+i|k^{\mathrm{l}})) + w^{\mathrm{l}}_{\mathrm{slack}} \cdot \|\mathrm{diag}(\boldsymbol{w}^{\mathrm{l}}_{\boldsymbol{\rho}}) \cdot \boldsymbol{\rho}^{\mathrm{l}}(k^{\mathrm{l}}+1+i|k^{\mathrm{l}})\|_1 + \|S_{\mathrm{ref}}(k^{\mathrm{l}}+i|k^{\mathrm{l}}) - S_{\mathrm{h}}(k^{\mathrm{l}}+1+i|k^{\mathrm{l}})\|_1) \tag{3-22}$$

s.t. MLD system dynamics, (2-30), (3-23a)

$$\boldsymbol{x}^{\min} - \boldsymbol{\rho}^{\mathrm{l}}(k^{\mathrm{l}}+1+i|k^{\mathrm{l}}) \leq \boldsymbol{x}(k^{\mathrm{l}}+1+i|k^{\mathrm{l}}) \leq \boldsymbol{x}^{\max} + \boldsymbol{\rho}^{\mathrm{l}}(k^{\mathrm{l}}+1+i|k^{\mathrm{l}}), \tag{3-23b}$$

$$\boldsymbol{v}^{\min} \leq \boldsymbol{v}(k^{\mathrm{l}}+i|k^{\mathrm{l}}) \leq \boldsymbol{v}^{\max}, \tag{3-23c}$$

$$0 \leq \boldsymbol{\rho}^{\mathrm{l}}(k^{\mathrm{l}}+i|k^{\mathrm{l}}) \leq \boldsymbol{\rho}^{\max}, \tag{3-23d}$$

$$\forall i \in \mathbb{Z}_{[0,N^{\mathrm{l}}-1]}, \tag{3-23e}$$

which is defined by the objective function (3-22) and its optimisation constraints (3-23). Furthermore, the decision vector and vector containing slack variables are similar to the ones introduced at the HMPC problem.

3-4-3 Controller Coupling

Two controller coupling schemes will be discussed in this section, a linear interpolation and a heuristic variant. The goal is to divide the monthly ATES hot well state reference the upper-layer provided, and to transform this monthly reference into hourly reference values for the LL-MPC to track. The linear interpolation set point tracking fixes the intermediate reference at each time step within that month to a linear interpolation from the initial storage state to the end value of the storage, i.e. the reference. This means that at each time step, the same amount of heat has to be stored for the duration of a month. This implementation may clash with the Power-to-X principles to utilise excess energy into other energy carriers. Therefore another approach may be the introduction of a proportional scaling factor for each time step within that month based on Power-to-X principles. This would mean that in months that heat energy has to be stored, a scaling factor based on PV generation may provide such a goal. In the colder months, when the ATES system supplies heat, the reference may be proportionally scaled by the thermal energy demand forecasts.

Naming the linear interpolation controller HiMPC - Linear and the scaled approach HiMPC - Heuristic, these working principles are compared for a year in Figure 3-7. Note that the reference trajectory is only plotted once since both simulations have identical references. Figure 3-8 shows a more detailed insight into the working principles of both controllers for some summer days. This figure shows that the HiMPC - Heuristic controller stores heat proportionally to solar power availability. Figure 3-9 illustrates the reference implementation for three winter days, where we see that more heat is extracted when there is a higher demand.

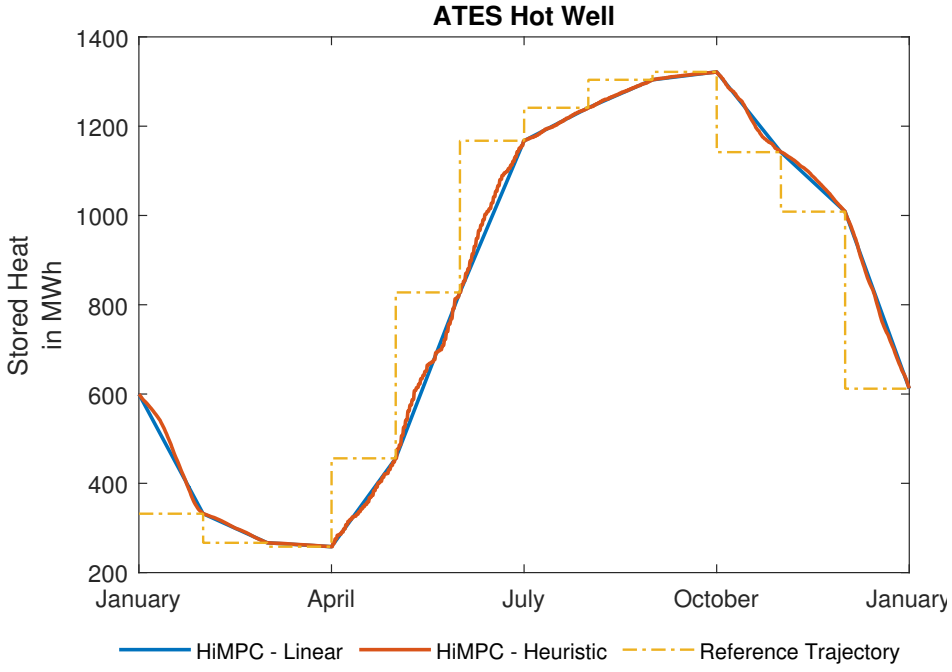

Figure 3-7: Comparison of the thermal energy storage of the ATES warm well for a year.

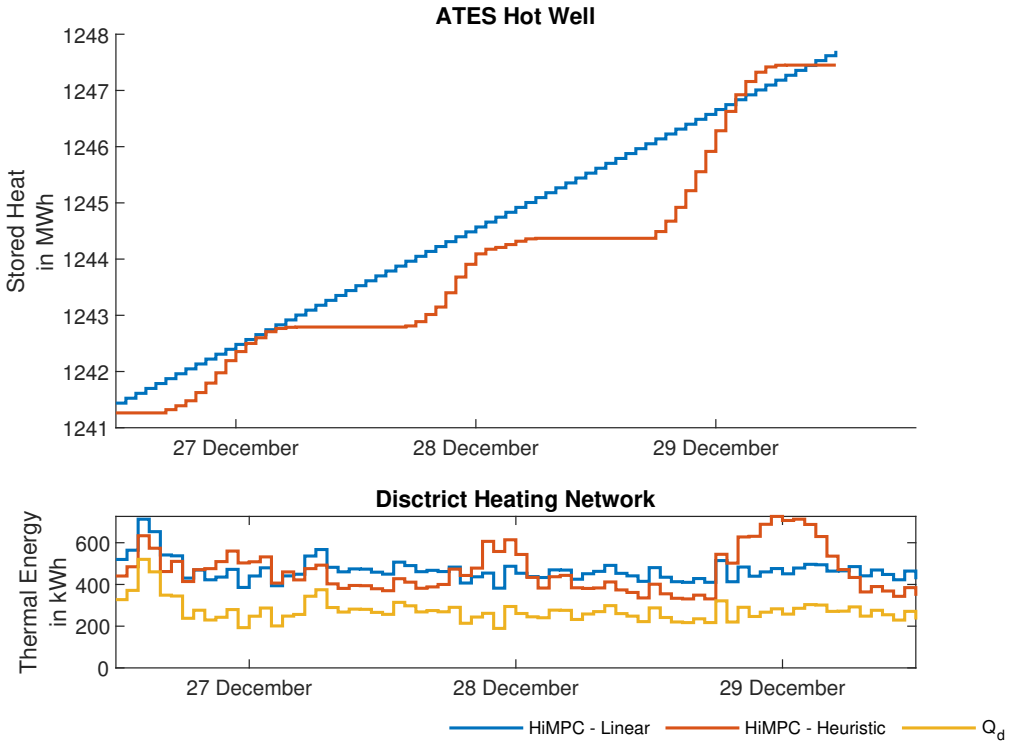

Figure 3-8: Comparison of the district heating system in the summer, where the HiMPC - Heuristic controller is driven by PV generation.

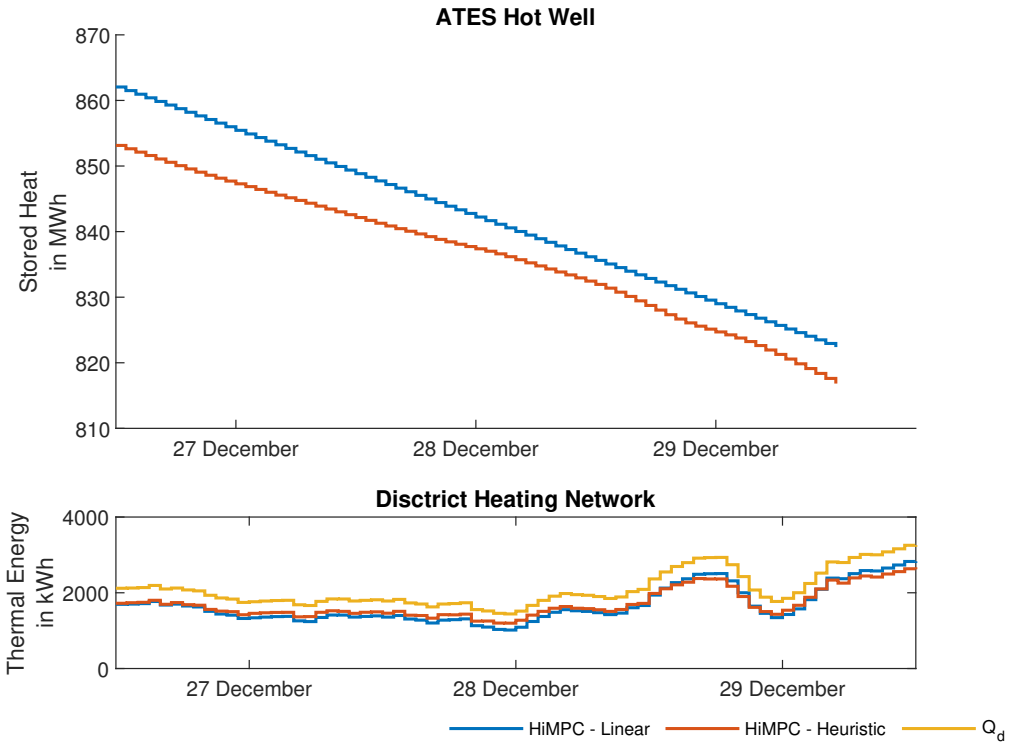

Figure 3-9: Comparison of the district heating system in the winter, where the HiMPC - Heuristic MPC is driven by the heating demand.

The upper-layer problem is repeated at the start of every month. The computed input sequence of the first time step is implemented on the ATES system model (2-17), and the prediction $S_{\mathrm{h}}^{*}(k^{\mathrm{u}}+1|k^{\mathrm{u}})$ serves as the reference for the LL-MPC. The two variants discussed are:

1. **Linear Interpolation:** This is the simplest method to deal with the reference of the upper-layer problem, and has also been used in the literature [53]. The principle is to interpolate linearly between the current state of the ATES hot well $S_{\mathrm{h}}(k^{\mathrm{l}})$ and final ATES state $S_{\mathrm{h}}^{*}(k^{\mathrm{u}}+1|k^{\mathrm{u}})$ to be reached at the end of the month. The following reference calculation is repeated at every time step k^{l}:

$$S_{\mathrm{ref}}(k^{\mathrm{l}}+i|k^{\mathrm{l}}) = S_{\mathrm{h}}(k^{\mathrm{l}}|k^{\mathrm{l}}) + \frac{i+1}{720\cdot k^{\mathrm{u}} - k^{\mathrm{l}}} \cdot (S_{\mathrm{h}}^{*}(k^{u}+1|k^{u}) - S_{\mathrm{h}}(k^{\mathrm{l}}|k^{\mathrm{l}})) \tag{3-24}$$
$$\forall i = 0,\ldots,N^{\mathrm{l}}-1$$

2. **Heuristic Assignment:** This method achieves to fully employ the Power-to-X principles for heat generation. As mentioned before, the principle is to divide the solar power at each time step $E_{\mathrm{pv}}(k^{\mathrm{l}})$ by the total solar power in that month, i.e $E_{\mathrm{pv}}(k^{\mathrm{u}})$. Therefore, heat for storage purposes will be generated using solar energy only. However, this rule only applies for months when heat is generated and stored, i.e. $S_{\mathrm{h}}^{*}(k^{\mathrm{u}}+1|k^{\mathrm{u}}) > S_{\mathrm{h}}(k^{\mathrm{l}})$. Then the reference is calculated as follows:

$$S_{\mathrm{ref}}(k^{\mathrm{l}}+i|k^{\mathrm{l}}) = S_{\mathrm{h}}(k^{\mathrm{l}}|k^{\mathrm{l}}) + \frac{\sum_{j=0}^{i+1} E_{\mathrm{pv}}(k^{\mathrm{l}}+j|k^{\mathrm{l}})}{E_{\mathrm{pv}}(k^{u})} \cdot (S_{\mathrm{h}}^{*}(k^{\mathrm{u}}+1|k^{\mathrm{u}}) - S_{\mathrm{h}}(k^{\mathrm{l}}|k^{\mathrm{l}})) \tag{3-25}$$
$$\forall i = 0,\ldots,N^{\mathrm{l}}-1$$

   For months when heat is utilised, i.e. in the winter, another reference update rule is developed. Now, the storage depletion is steered by the amount of heating demand. At every time step k^{l} the following equation is used to update the hourly references:

$$S_{\mathrm{ref}}(k^{\mathrm{l}}+i|k^{\mathrm{l}}) = S_{\mathrm{h}}(k^{\mathrm{l}}|k^{\mathrm{l}}) + \frac{\sum_{j=0}^{i+1} Q_{\mathrm{d}}(k^{\mathrm{l}}+j|k^{\mathrm{l}})}{Q_{\mathrm{d}}(k^{u})} \cdot (S_{\mathrm{h}}(k^{\mathrm{l}}|k^{\mathrm{l}}) - S_{\mathrm{h}}^{*}(k^{\mathrm{u}}+1|k^{\mathrm{u}})) \tag{3-26}$$
$$\forall i = 0,\ldots,N^{\mathrm{l}}-1$$

3-5 Dealing with Uncertainties

When considering uncertainties acting on Power-to-X systems, one may think of uncertainties introduced by the stochastic nature of atmospheric processes, uncertain demands, prices, imperfect measurements of initial conditions, and modelling errors. In this thesis uncertainties induced by exogenous disturbances will be considered, i.e. uncertain generation, demands and prices. These disturbances acting on the system for the case study in this thesis were investigated in Section 2-3. This section also dealt with the design of persistence methods for forecasting of the exogenous disturbances. Let us now introduce the following decomposition for the actual disturbance:

$$\omega(k) = \bar{\omega}(k) + \hat{\omega}(k) \tag{3-27}$$

where $\bar{\omega}(k)$ is the nominal part of the disturbance provided by forecast (e.g. load demand or photovoltaic (PV) generation) and $\hat{\omega}(k)$ is the stochastic prediction error at each time step k. Generally, the stochastic part is either modelled as a discrete variable with an assumed distribution [26], or as a bounded uncertainty.

3-5-1 Deterministic Framework

The main assumption of deterministic MPC to cope with uncertainties relies on the so-called certainty-equivalence property [26]. Subsequently, the resulting deterministic MPC controller is often called certainty-equivalent MPC (CEMPC). In the setting of this thesis, it means that imperfect forecasts are assumed to be correct [22, 26–29]. A certainty-equivalence strategy to deal with disturbances is reducing the disturbance vector to its expected value with $\hat{\omega}(k) = 0$„ i.e.

$$\boldsymbol{\omega}(k) = E\left(\bar{\boldsymbol{\omega}}(k)\right), \tag{3-28}$$

where $\boldsymbol{\omega}(k)$ is the real disturbance vector, $\bar{\boldsymbol{\omega}}$ is the predicted disturbance vector, and $E[\cdot]$ is the expectation operator. Alternatively, other certainty-equivalent strategies may include choosing $\boldsymbol{\omega}(k)$ as the value with maximum probability, as a random sample of $\boldsymbol{\omega}(k)$ or as a nominal value. The disturbance realisation in the prediction horizon of the MPC cycle can be compactly written as:

$$\tilde{\boldsymbol{\omega}}(k) = \begin{bmatrix} (\boldsymbol{\omega}(k|k))^T & \dots & (\boldsymbol{\omega}(k+N-1|k))^T \end{bmatrix}^T \tag{3-29}$$

Generally, deterministic MPC on a stochastic system leads to average-performing systems, and guarantee no constraint satisfaction. Consequently, this would mean that in the case of large constraint violations, the computed control input has to be recomputed within the controller time interval by a recovery strategy. In the setting of this thesis, it would mean that we must assume that the heat pump and utility grid interaction may react fast enough to ensure thermal and electrical energy balance satisfaction. The necessity of a recovery strategy may greatly reduce the economic operation of the system. The practical implementation of this framework is discussed in Section 4-1.

3-5-2 Stochastic Framework

In the stochastic MPC (SMPC) framework, a chance-constrained optimisation problem is solved [54]. These are obtained by the substitution of constraints, by chance constraints, i.e.

$$P\left[g(x(k), u(k)) \leq 0\right] \geq 1 - p, \tag{3-30}$$

which allows for some degree of constraint violation bounded by a predefined 'violation risk', p and, generally by replacing the objective function by the expectation of the objective function. Nowadays, there exist many methods and extensions on stochastic MPC [54]. This thesis will only cover a randomised method, called scenario-based MPC [37].

Randomised approaches are founded on the assumption that several scenarios with possible evolutions of the disturbance are known, i.e. $(\tilde{\boldsymbol{\omega}}(k))^{(j)}$, with superscript j denoting the jth scenario. These approaches' main idea is to reformulate the problem for a finite number of scenarios, sufficient enough to reformulate the stochastic optimisation problem into a tractable deterministic problem. The sufficient number of scenarios is based on the following condition:

$$N_{\mathrm{s}} \geq \frac{2}{p}\left(\ln\frac{1}{\beta} + d\right) \tag{3-31}$$

that guarantees constraints such as (3-30) lead to feasible solutions, with a confidence level $(1-\beta)$ with β a user-defined parameter [55]. However, most constraints due to scenarios are redundant. Therefore, the following implementation is used [37]:

$$\max_{j=1,\ldots,N_{\mathrm{s}}} (\tilde{\boldsymbol{\omega}}(k))^{(j)}, \tag{3-32}$$

where N_{s} is the number of scenarios and the max operator applies element-wise.

In the setting of this thesis, the uncertain PV generation E_{pv} and heating demand Q_{d} will be implemented as their scenario realisations. The remaining exogenous disturbances do not affect the system as much as the earlier mentioned PV generation and heating demand. The forecasting errors of the solar power generation and heat demand are fitted with a kernel distribution, see Figure 3-10 for heat demand. This choice was based on the histograms of the errors. It appears that these do not come from any obvious distribution, so the kernel distribution was fit to nonparametrically estimate the probability density function of the errors.

Scenarios will be generated by randomly sampling errors from the inverse empirical cumulative distribution function with a random variable $(0, 1)$ from a uniform distribution. These sampled errors and the point forecasts are used to calculate the scenarios by employing (3-27). Then a desired number of scenarios is generated and reduced through probability matching, see Figure 3-11. This figure shows 20 scenario realisations for the heating demand for a day, along with the real demand and the forecast. Furthermore, (3-32) is used for implementation in the optimal control problem. Note that for PV generation (3-32) is reformulated as an element-wise minimum.

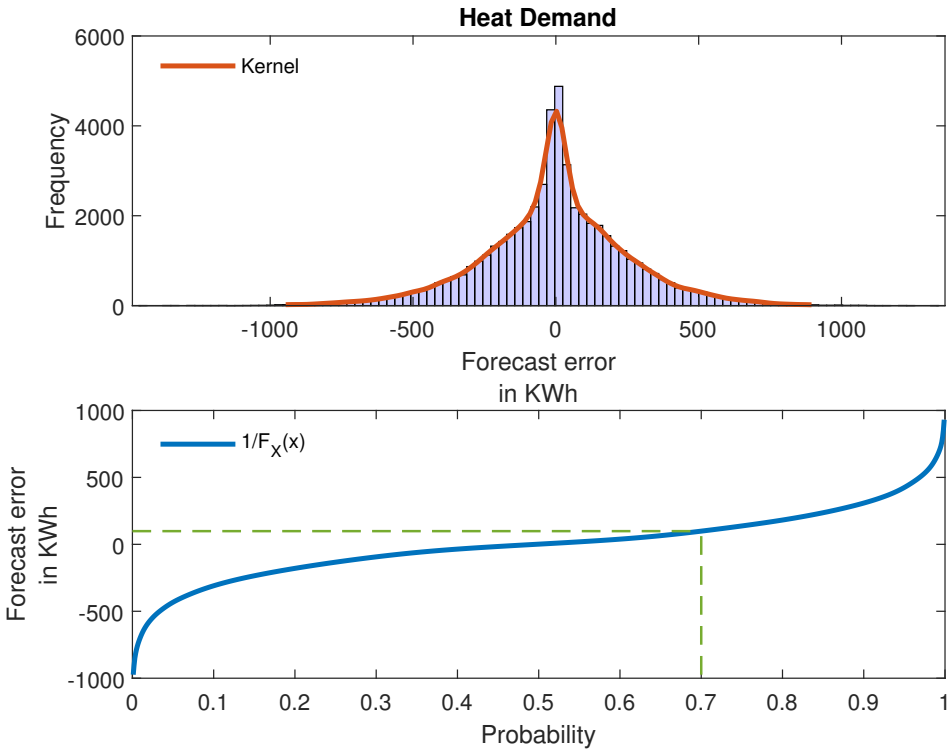

Figure 3-10: PDF heat demand forecast error and inverse CDF, dashed in green is a sample from a uniform distribution and corresponding error sample.

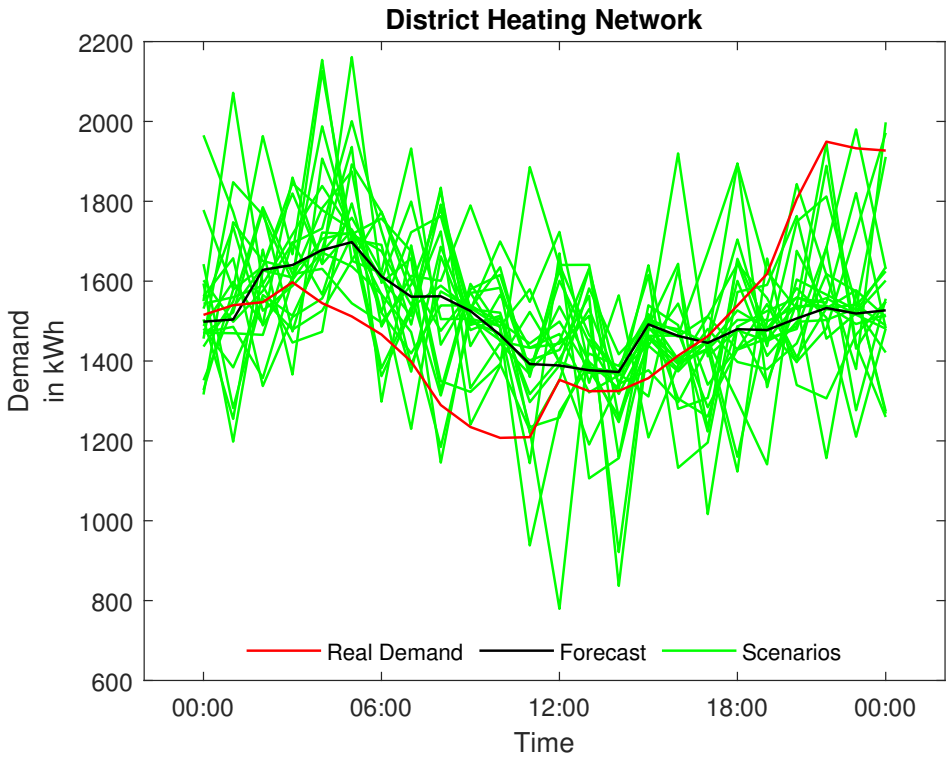

Figure 3-11: Scenario generation example for heat demand.

Chapter 4

Case Study: Hierarchical MPC for a Power-to-X Concept

This Chapter performs a simulation of a year for the case study of the Power-to-X system described in Section 2-2. First, the simulation setup will be given in Section 4-1 along with all prerequisites for its implementation. Then, in Section 4-2 a basis is formed for assessing the proposed controllers in Chapter 3. At last, in Section 4-3 the simulation results are illustratively presented along with controller performance metrics.

4-1 Introduction

The controllers assessed as the Energy Management System (EMS) of the Power-to-X case study provide hourly set-points for the low-level controllers at the corresponding unit in the system. This chapter aims to compare Model Predictive Control (MPC) controllers presented in Chapter 3 by simulation with historical data of the year 2013. We will only consider certainty-equivalent MPC (CEMPC) and scenario-based MPC in the comparison since these are the only control methods that can be implemented in reality. Additionally, a rule-based controller and prescient MPC (PMPC) controller will be introduced to assess the theoretical and practical potentials of the following control schemes:

- **Heuristic Model Predictive Control (HMPC):** The single-layer MPC scheme based on heuristic rules (Algorithm 1) and optimal control problem characterised by objective (3-17) and constraints (3-18a)-(3-18d);
- **Hierarchical Model Predictive Control (HiMPC) - Linear:** Two-layered control scheme characterised by an upper-layer MPC (UL-MPC) ((3-20) and (3-21)) and lower-layer MPC (LL-MPC) ((3-22) and (3-23)). The reference is calculated by linear interpolation, i.e. (3-24);

- **Hierarchical Model Predictive Control (HiMPC) - Heuristic:** Attempt to improve the linear interpolation variant of the HiMPC scheme given by using update rules (3-25) or (3-26).

The constants, parameters and optimisation variables are presented in Table 4-1 along with their respective bounds and units. Due to the addition of slack variables in the optimal control problem, we may assume that constraint violations will occur. When a constraint is violated in the electricity system, we assume that the utility grid will compensate for any imbalances. When the imbalance causes more electricity to be exported than the lower bound value $P_{\text{grid}}^{\min} = -4500\,\text{kW}$, the excess is curtailed, i.e. no economic benefit. We assume this curtailment occurs in the inverter of the photovoltaic (PV) installation. On the other hand, power imports larger than the utility grid limit will be charged double.

Furthermore, we assume that the heat pump can react fast enough to compensate for heat demand/supply imbalances. Regarding the demineralised water and hydrogen systems, we impose a conservative lower bound to the storage systems to ensure imbalance prevention, i.e.:

$$x_{\text{hy}}^{\min} = H_{\text{d}}^{\max} \tag{4-1}$$

$$x_{\text{dw}}^{\min} = F_{\text{d}}^{\max}, \tag{4-2}$$

where superscripts $^{\min}$ and $^{\max}$ denote the minimum and maximum values. Furthermore, H_{d} and F_{d} are hydrogen and demineralised water demands, respectively. The lower and upper bounds can be found in Table 4-1. When the upper limits of the hydrogen and demineralised water storages are exceeded, the excess will be dissipated. Moreover, the battery energy storage system (BESS) requires a lower bound of at least 10 per cent of its maximum capacity, i.e.

$$x_{\text{b}}^{\min} = 0.1 \cdot x_{\text{b}}^{\max}, \tag{4-3}$$

this constraint is imposed to limit the BESS life time detoriation.

The optimisation problems to be solved were formulated as Mixed Integer Linear Programming (MILP) problems. Hence the GUROBI solver is used along with the YALMIP toolbox [56] in MATLAB 2019a.

Symbol	Description	Value/Bounds	Units
	States		
x_{b}	Battery State of Charge	$\begin{bmatrix} 500 & 5000 \end{bmatrix}$	kWh
$\boldsymbol{x}_{\mathrm{a}}$	Thermal energy content warm and cold well	$\begin{bmatrix} 0 & 3 \end{bmatrix}$	MWh
x_{hy}	Content hydrogen storage	$\begin{bmatrix} 0 & 200 \end{bmatrix}$	kg
x_{dw}	Volume demineralised water storage	$\begin{bmatrix} 0 & 150 \end{bmatrix}$	m^3
	Decision Variables		
P_{b}	Energy to or from BESS	$\begin{bmatrix} -1650 & 1650 \end{bmatrix}$	kWh
P_{grid}	Energy imported or exported	$\begin{bmatrix} -4500 & 4500 \end{bmatrix}$	kWh
Q_{hp}	Heat output of heat pump	$\begin{bmatrix} 0 & 9000 \end{bmatrix}$	kWh
u_{a}	Water volume pumped from ATES wells	$\begin{bmatrix} -75 & 75 \end{bmatrix}$	m^3
H_{el}	Hydrogen produced by the electrolyser	$\begin{bmatrix} 0 & 25 \end{bmatrix}$	kg
H_{trade}	Hydrogen imported or exported	$\begin{bmatrix} -25 & 25 \end{bmatrix}$	kg
F_{ro}	Volume of demineralised water purified by reverse osmosis	$\begin{bmatrix} 0 & 150 \end{bmatrix}$	m^3
$\boldsymbol{\rho}$	Slack variables	-	-
	MLD Decision Variables		
z_{b}	Auxiliary variable, $z_{\mathrm{b}} = \delta_{\mathrm{b}} P_{\mathrm{b}}$	$\begin{bmatrix} 0 & 1650 \end{bmatrix}$	kWh
δ_{b}	Binary variable, BESS	$\{0, 1\}$	-
$\boldsymbol{z}_{\mathrm{a}}$	Auxiliary variable, heat system	$\begin{bmatrix} -3000 & 3000 \end{bmatrix}$	kWh
$\boldsymbol{\delta}_{\mathrm{a}}$	Binary variable, heat system	$\{0, 1\}$	-
	Disturbances		
E_{pv}	Solar energy generation	$\begin{bmatrix} 0 & 9000 \end{bmatrix}$	kWh
Q_{d}	District heating demand	$\begin{bmatrix} 100 & 3.5 \cdot 10^3 \end{bmatrix}$	kWh
H_{d}	Hydrogen demand	$\begin{bmatrix} 0 & 26 \end{bmatrix}$	kg
F_{d}	Demineralised water demand	$\begin{bmatrix} 0 & 12 \end{bmatrix}$	m^3
	Constants		
η_{b1}	Battery storage loss efficiency	1	-
η_{ch}	Battery charging efficiency	0.95	-
η_{dch}	Battery discharging efficiency	1/0.95	-
η_{a}	ATES heat loss	$0.95^{1/720}$	-
α_{h}	Thermal power coefficient warm well	39.8	$\mathrm{kWh/m}^3$
α_{c}	Thermal power coefficient cold well	3.5	$\mathrm{kWh/m}^3$
$\eta_{\mathrm{el,dw}}$	Conversion efficiency from demineralised water to energy needed	0.191	$\mathrm{m}^3/\mathrm{kWh}$
$\eta_{\mathrm{dw,hy}}$	Conversion efficiency from hydrogen to demineralised water	13.75	m^3/kg
$c_{\mathrm{hy,im}}$	Importing price hydrogen per kilogram	10	€/kg
$c_{\mathrm{hy,im}}$	Exporting price hydrogen per kilogram	6	€/kg

Table 4-1: States, decision variables, disturbances and constants with their unit, respective bounds and values.

4-2 Controller Assessment

4-2-1 Benchmark: Rule-Based Control

A Rule-Based Controller (RBC) will be used as a performance benchmark to compare the proposed MPC controllers against. Such a controller acts directly as the EMS and exists of if-else statements based on available information within a single control time interval. The RBC will not make use of predictions within its decision-making process. In its simplest form as developed for this thesis, the RBC makes its decision to generate, produce or import when a certain lower-limit threshold is passed, e.g. (4-1) or (4-2). Moreover, the main principle of this controller is to utilise excess power into heat. The main principles of the developed RBC for this thesis are given by Algorithm 2 in Appendix B.

4-2-2 Theoretical Potential: Prescient MPC

PMPC is when a given MPC framework is simulated with full knowledge of future disturbances. Hence such a controller can be used to assess the theoretical potential of an MPC scheme when compared to the RBC. Furthermore, such PMPC is also used to determine the slack variable minimisation weights, which are summarised in Table 4-2. First of all, the ATES system states trajectories, do most of the time, not operate close to their bounds. Therefore, the slack variables corresponding to the ATES states are relatively small. Furthermore, the hydrogen storage tends to show constraint violations relatively quick, which is why the slack variable corresponding to the hydrogen storage is relatively large.

Controller	States	$\boldsymbol{w}_\rho$	w_{slack}
HMPC	$\begin{bmatrix} x_{\text{b}} & \boldsymbol{x}_{\text{a}}^T & x_{\text{el}} & x_{\text{dw}} \end{bmatrix}^T$	$\begin{bmatrix} 1 & 0.1 & 0.1 & 10 & 1 \end{bmatrix}^T$	1
LL-MPC	$\begin{bmatrix} x_{\text{b}} & \boldsymbol{x}_{\text{a}}^T & x_{\text{el}} & x_{\text{dw}} \end{bmatrix}^T$	$\begin{bmatrix} 1 & 0.1 & 0.1 & 10 & 1 \end{bmatrix}^T$	0.1
UL-MPC	$\boldsymbol{x}_{\text{a}}$	$\begin{bmatrix} 1 & 1 \end{bmatrix}^T$	0.01

Table 4-2: Weighing parameters for the slack variable minimisation for each proposed MPC controller.

4-2-3 Performance Indices

The MPC schemes compared in this case study will be assessed according to the following performance indices:

- **Yearly Revenue:** This performance index is directly implemented within the control objective function of the MPC controllers. This metric is calculated by summing C_{grid} and C_{hy} over a year of simulation;
- **Practical Potential:** The practical potential is the percentage gain of the yearly revenue against the RBC;

- **Theoretical Potential:** The theoretical potential of the controllers is the percentage gain of the yearly revenue of the PMPC against the RBC's yearly revenue;
- **Carbon Dioxide Emission Savings:** The emission savings metric is not directly incorporated in the objective function. However, it is still an important metric to look at and is calculated by i.e., (3-8);
- **Heat Storage:** This metric looks at the amount of thermal energy left in the ATES hot well. Since this heat may be used in the future this metric represents an economic value.

4-3 Results

The performance metrics for the proposed control strategies for a simulation of the year 2013 are given in Table 4-3. Since the performance metric of operational expenses is explicitly incorporated in the cost, this metric should be actually compared. Note that all controllers are tuned for maximum yearly revenue. The HiMPC - Heuristic controller in the deterministic framework performs best on economic cost optimisation, followed by its stochastic counterpart. What we observe is that the deterministic controllers are more aggressive in terms of constraint violations, whereas scenario-based MPC controllers are more conservative. This conservativeness is also seen in the yearly revenue of the scenario-based MPC controllers, which perform less compared to the deterministic counterparts. Furthermore, almost all simulations end with a comparable amount of heat left in the ATES hot well, except for the deterministic HMPC controller.

Control Strategy	**HMPC**		**HiMPC - Linear**		**HiMPC - Heuristic**	
	CEMPC	SMPC	CEMPC	SMPC	CEMPC	SMPC
Yearly Revenue in € (practical potential)	$1.74 \cdot 10^5$ (84.59%)	$1.56 \cdot 10^5$ (65.50%)	$2.19 \cdot 10^5$ (132.33%)	$1.73 \cdot 10^5$ (83.54%)	$\mathbf{2.22 \cdot 10^5}$ **(135.52%)**	$2.12 \cdot 10^5$ (124.91%)
Emission Savings in tonnes	$4.37 \cdot 10^2$	$3.44 \cdot 10^2$	$3.29 \cdot 10^2$	$3.29 \cdot 10^2$	$3.73 \cdot 10^2$	$2.92 \cdot 10^2$
Heat Storage in MWh	0.293	0.611	0.626	0.612	0.626	0.627
Constraint Violations	13.52%	9.33%	7.63%	7.13%	7.59%	6.89%

Table 4-3: Comparison of control strategies based on performance indices.

Figure 4-1 compares the ATES hot well utilisation for each proposed controller presented in the deterministic and stochastic framework. As highlighted before, we see the working principles of both HiMPC controllers; this time, however, the HiMPC - Heuristic controller may not always reach the setpoint provided by the upper-layer controller due to forecast inaccuracy. The linear interpolation variant is less sensitive to the forecast errors on the system since time is certain. Moreover, comparing the HiMPC controllers for the stochastic and deterministic frameworks no evident differences are present. The reason for this is that the recovery strategies for both control frameworks ensure that the references are reached. Looking at the HMPC controllers' storage trajectories we must note that these controllers are tuned for maximum revenue, and not for resemblance to the HiMPC controllers.

Other simulation results will be illustratively assessed for three days in July 2013. The energy flows in the microgrid are depicted in Figure 4-2 and Figure 4-3 for the CEMPC and SMPC

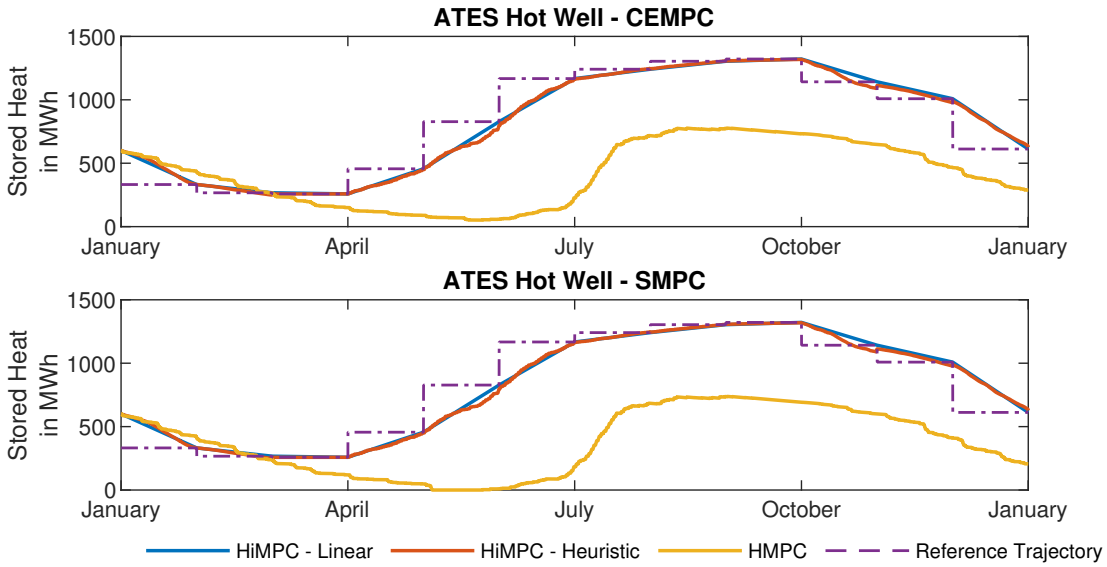

Figure 4-1: Simulation result of the ATES hot well utilisation for one year.

controllers, respectively. To assess the microgrid energy flows, we introduce a new variable, the utilised energy, i.e.

$$P_{\mathrm{u}}(k) = P_{\mathrm{hp}}(k) + P_{\mathrm{ro}}(k) + P_{\mathrm{el}}(k), \tag{4-4}$$

where $P_{\mathrm{u}}(k)$ is the utilised power, $P_{\mathrm{hp}}(k)$ the power to the heat pump, $P_{\mathrm{ro}}(k)$ power utilised for the reverse osmosis process and $P_{\mathrm{el}}(k)$ the power to the electrolyser system. We can observe that the battery is filled up during the day, and is discharged during the night for constant energy utilisation. The electrolyser's power input is most of the time maximised because it is most efficient operating at maximum capacity. Furthermore, the HiMPC - Heuristic has peaks of energy utilisation during the day accounted for by the heat production during those times. Most of the time there is too much excess energy. Therefore some generated energy still has to be exported during the day, sometimes even leading to curtailments. During the simulation, we have never experienced an upper-bound violation of the grid capacity P_{grid}, therefore no controller has faced adverse penalties. Furthermore, when the BESS had exceeded its limits, the utility grid had restored the storage's energy to that limit, i.e. no windup effects.

Figure 4-4 and Figure 4-5 give more insight about storage utilisation in the system for the deterministic and stochastic frameworks, respectively. We may directly observe that the battery and demineralised water storages are filled up during the day to utilise in the night times. Hence all controllers have made smart decisions about utilising energy for storage purposes when there is 'free' solar energy available. Furthermore, some constraint violations occur, however these are anticipated for by the conservative lower bounds. What is also directly visible from these figures is that the amount of hydrogen in the storage is never at full capacity. Therefore, one may suggest reducing the total capacity of the hydrogen storage to limit expenses.

Control Strategy	**HMPC** PMPC	**HiMPC - Linear** PMPC	**HiMPC - Heuristic** PMPC
Yearly Revenue in € (theoretical potential)	$2.49 \cdot 10^5$ (164.17%)	$3.00 \cdot 10^5$ (218.27%)	$\mathbf{3.44 \cdot 10^5}$ (264.95%)
Emission Savings in tonnes	$4.25 \cdot 10^2$	$6.32 \cdot 10^2$	$8.50 \cdot 10^2$
Heat Storage in MWh	0.325	0.613	0.612

Table 4-4: Comparison of PMPC control to assess the theoretical potential of each controller.

Table 4-4 shows the results for the same simulation set up for PMPC when full knowledge of disturbances are available. These results give us an insight into the theoretical potential of the control schemes that are designed. Again the HiMPC - Heuristic controller is the best performing based on economic cost and emission savings. However, when we compare the PMPC and CEMPC counterparts of the HiMPC - Heuristic controller, we conclude that this control scheme suffers most from uncertainties regarding the economic objective.

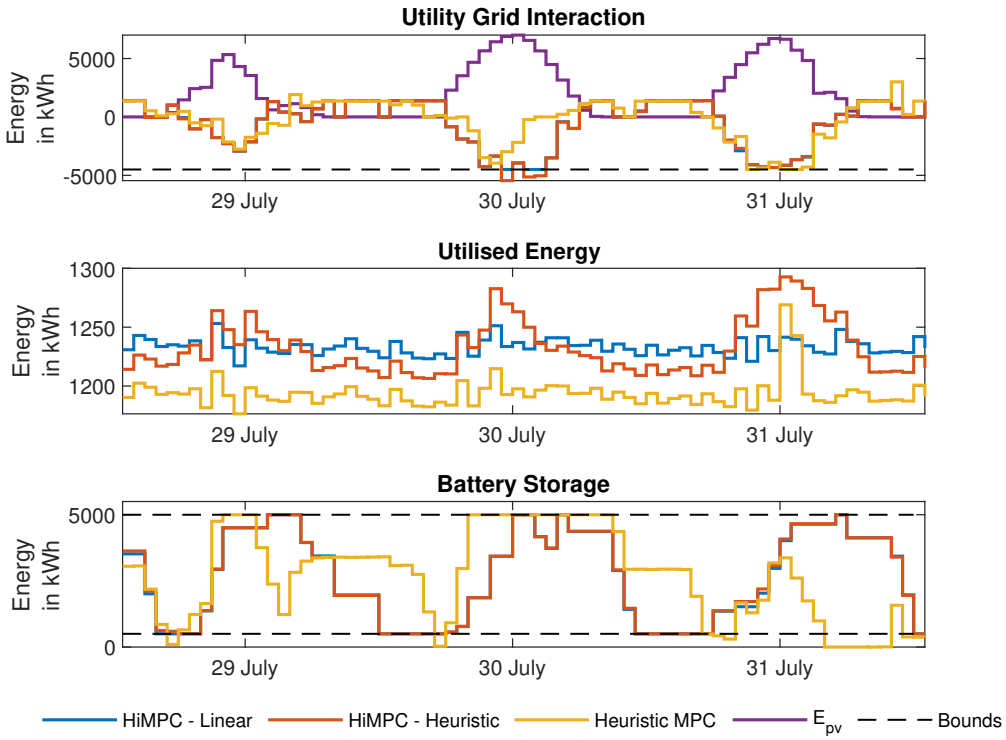

Figure 4-2: Microgrid energy flows, utilised energy and battery storage dynamics for several days in the summer for controllers in the deterministic framework

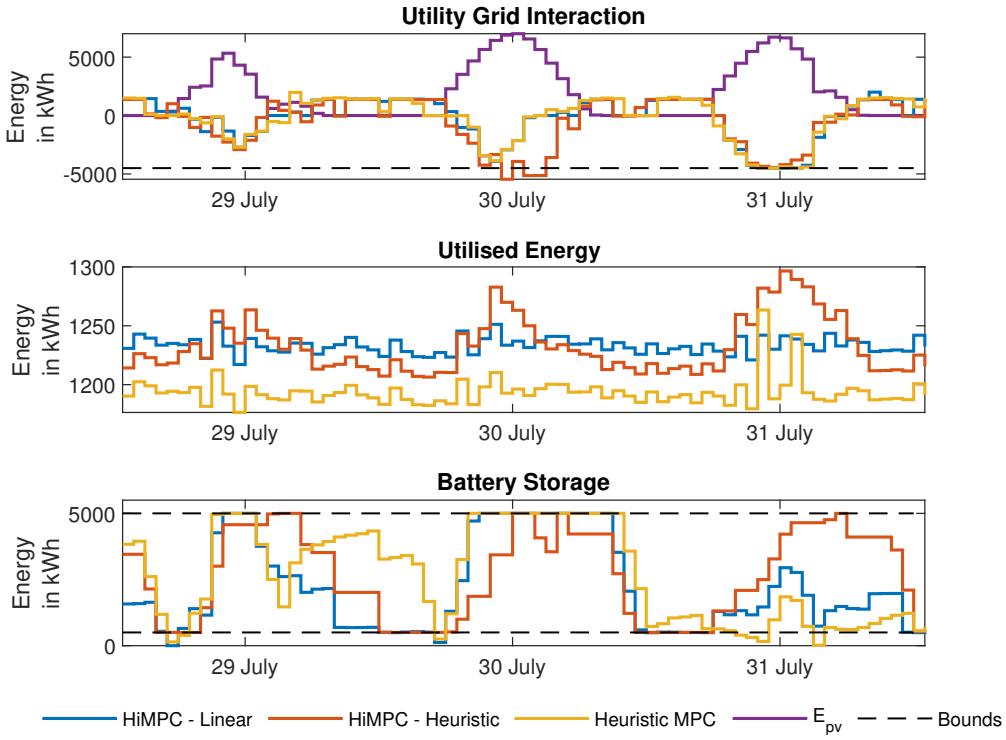

Figure 4-3: Microgrid energy flows, utilised energy and battery storage dynamics for several days in the summer for controllers in the stochastic framework

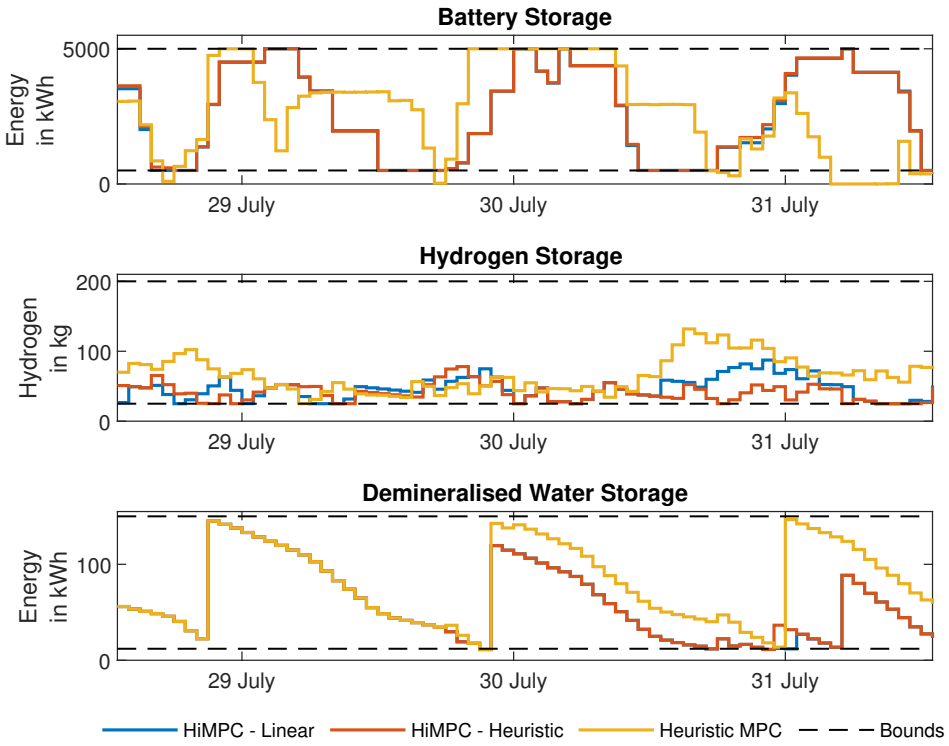

Figure 4-4: Storage utilisation comparison for the deterministic MPC framework.

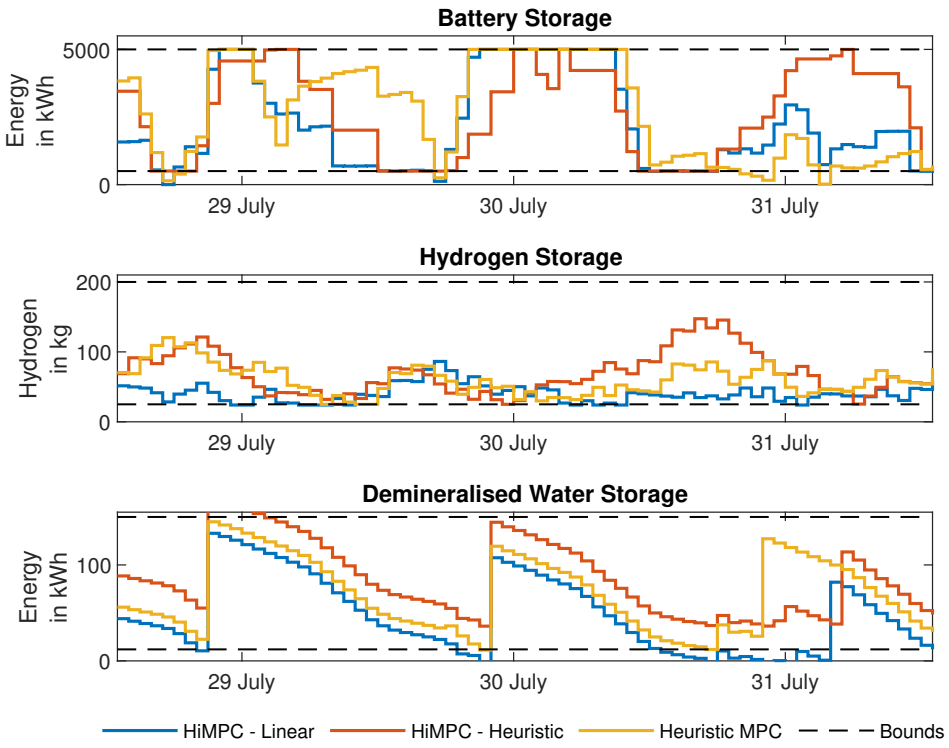

Figure 4-5: Storage utilisation comparison for the stochastic MPC framework.

Chapter 5

Conclusions and Recommendations

5-1 Summary

The idea behind the Power-to-X system comes from the intermittency of RES and the discrepancy between the generation and demand of energy carriers within a system. The physical system of Power-to-X setup is generally a microgrid extended with the availability of multiple energy carriers, resulting in a Multi-Energy System (MES). The Power-to-X principle is to utilise the excess of generated electrical energy at a particular time into another energy carrier, i.e. hydrogen (Power to Gas) or heat (Power to Heat). Therefore such a system provides load flexibility and synergy effects between multiple energy carriers. Furthermore, temporal discrepancies can be solved since energy carriers such as heat or gasses may be stored for long periods quite efficiently in contrast to electrical energy.

The Power-to-X system concept studied in this thesis consists of electrical energy, thermal energy, hydrogen for mobility and water. The goal of this research was to investigate the economic viability of this system based on a case study. This case study was supported by simulation with historical data from the Netherlands. The system under consideration allows for electricity and hydrogen imports and exports. Moreover, all energy carriers can be stored and utilised within short periods, increasing flexibility. Though, thermal energy may only be stored for larger periods of time in the seasonal storage, the Aquifer Thermal Energy Storage (ATES). The dynamics of the storage elements were modelled and concatenated into an overall Mixed Logical Dynamical (MLD) model, capturing both continuous and binary states and inputs. This modelling decision was necessary to capture 'operating modes' of the storage elements, for instance charging or discharging of the battery energy storage system (BESS).

The Power-to-X system's energy flow decisions are made by the Energy Management System (EMS). The EMS decides the amount of energy to or from storage elements, importing and exporting decisions, generator deployment, etc. The MPC framework was chosen for serving the role of the EMS of the Power-to-X system. First, decisions about the forecast of exogenous disturbances were made. After some analysis, appropriate persistence models for

each of the exogenous disturbance acting of the system were formulated. The first approach to deal with the temporal discrepancy within the system was the development of a Heuristic Model Predictive Control (HMPC) scheme. This controller incorporated heuristics in the form of a terminal objective function. This objective serves the purpose of incorporating the economic value of heat when used some months ahead. Another approach to solving the energy management problem of the case study was by some temporal decomposed optimisation formulation. This solution took the form of a two-layered Hierarchical Model Predictive Control (HiMPC) scheme. Where the lower-layer controller dealt with the 'regular' hourly EMS tasks, and the upper-layer was an anticipatory control problem for the long-term heat storage. The upper-layer's task was to sent computed 'optimal' references to the lower-layer to track.

The illustrative case study performed in this thesis was based on historical data from 2013. The proposed controllers were assessed within the deterministic and stochastic frameworks based on performance indices. The benchmark values for these performance indices were accessed from an Rule-Based Controller (RBC). These controllers were the HMPC controller and two variants of the HiMPC controller, a linear interpolation and a heuristic variant. The latter makes use of proportionally dividing the reference by the uncertain solar power availability or heat demand. The economically best performing controller was the HiMPC - Heuristic scheme implemented within the deterministic certainty-equivalence framework.

5-2 Conclusions

The illustrative case study for the conceptual Power-to-X system has led to some insights about its suitability for the Dutch energy-transition scenario. For the Power-to-X concept to fully exploit its fundamental principles, surplus energy had to be available in the grid. Therefore the first conclusion of the simulation is that there was enough surplus to fully employ the Power-to-X principles, based on 2013 historical data. What is also shown is that the excess was too significant, meaning that there was still a large amount of electricity export to the utility grid. This phenomenon only occurred when the BESS was at its full capacity. Therefore one may also consider increasing the BESS capacity or introducing a second electricity storage unit. Furthermore, it can be stated that the Power-to-X system brings a lot of flexibility in the microgrid since electricity was always utilised in any form of conversion, leading to more flexibility and less curtailment. These insights result to the second conclusion that the implementation of PV technology is highly beneficial for the Dutch scenario.

The case study also served to assess the economic viability of the presented Power-to-X system. The simulations of the proposed MPC schemes as EMS of the system, answer this question. Indeed, the Power-to-X system is deemed economically viable, at best, the system is approximated to have a payback time of 11.1 years. This result was achieved by the HiMPC - Heuristic control scheme in the deterministic framework. What has to be noted is that the deterministic framework yields better results, with the downside that the aggressive decisions result in more constraint violations of the grid capacity. What is significant to note is that the grid capacity for importing was never exceeded. Hence no adverse penalties on grid capacity violation were imposed on the controllers. What is important to note is that the more 'aggressive' deterministic controller may gather significant economical penalties in

a slightly different Power-to-X system setup. Moreover, we can state that the Power-to-X system leads to very compelling carbon dioxide emission savings, even when it is not directly optimised in the EMS' decisions.

The optimal control problem of the EMS is highly influenced by uncertainties in the forecast of exogenous disturbances. This is seen in the results when prescient MPC (PMPC) is compared to the approaches including uncertainties. For the best controller, the HiMPC - Heuristic, there is still as much as 55% to improve in yearly revenue, meaning it is highly susceptible to forecast errors. Therefore it is recommended to improve forecasting based on techniques presented in Section 2-3 or to resort to probabilistic forecast methods.

5-3 Future Work

This section lists the recommendations for future work.

1. In Figure 2-1 the first conceptual design of the Power-to-X system in the considered case study was illustrated. What is seen, but not implemented in the case study are the electrical demands and photovoltaic (PV) generation of the residential area. This is done intentionally because there are no tractable laws yet in the Netherlands to resupply electricity to a neighbourhood originating from a BESS, (partly) filled with electricity of that neighbourhood. Therefore to fully employ Power-to-X strategies and principles, new case studies may prove valuable when those laws exist.

2. An Aquifer Thermal Energy Storage (ATES) model was presented based on energy only and then extended to a Mixed Logical Dynamical (MLD) district heating model. Real measurements, or simulations did not validate this model. Furthermore, the application of MODFLOW, a simulation tool for ATES systems is recommended as future work.

3. The objective of the EMS in this thesis' case study was an economic one. This was done by explicitly minimising the operational expenses of the system. The resulting problems were a unit commitment problem and a dynamic energy dispatch problem. However, the same goal could also be attained or improved by implementing demand response techniques. This enables flexibility in the energy loads, resulting in a more significant decision space for the controllers.

4. The presented HiMPC schemes may be improved. A suggestion would be the implementation of event-driven updates of the upper-layer optimisation or faster update rates for this layer. These solutions would result in a more frequently updated reference layer for the lower-layers to track.

Appendix A

Detailed Model Derivation

A-1 Battery Energy Storage System (BESS) Dynamics

The Mixed Logical Dynamical (MLD) system matrices of the dynamic battery energy storage system (BESS) model (2-7a) are given by:

$$\begin{aligned}
\boldsymbol{E_{b1}} &= \begin{bmatrix} P_{\mathbf{b}}^{\max} & -(P_{\mathbf{b}}^{\max}+\epsilon) & P_{\mathbf{b}}^{\max} & P_{\mathbf{b}}^{\max} & -P_{\mathbf{b}}^{\max} & -P_{\mathbf{b}}^{\max} \end{bmatrix}^T, \\
\boldsymbol{E_{b2}} &= \begin{bmatrix} 0 & 0 & 1 & -1 & 1 & -1 \end{bmatrix}^T, \\
\boldsymbol{E_{b3}} &= \begin{bmatrix} 1 & -1 & 1 & -1 & 0 & 0 \end{bmatrix}^T, \\
\boldsymbol{E_{b4}} &= \begin{bmatrix} P_{\mathbf{b}}^{\max} & -\epsilon & P_{\mathbf{b}}^{\max} & P_{\mathbf{b}}^{\max} & 0 & 0 \end{bmatrix}^T,
\end{aligned}$$

where $P_{\mathbf{b}}^{\max}$ is the maximum value of BESS power P_{b} and ϵ denotes the machine precision.

A-2 Heat System Model Derivation

The district heating system consists of a heat pump for thermal energy generation and an Aquifer Thermal Energy Storage (ATES) for long-term thermal energy storage. The system's goal is to ensure the Power-to-X system's heating demands. The district heating system model was based on the assumptions of constant ATES well temperatures and constant ambient temperature. Hence based on these three temperatures, there are three constant power coefficients, α_{h}, α_{c} and $\alpha_{\mathrm{amb}} = 0$. Consequently, total power coefficient α could take the values of $\alpha_1 = \alpha_{\mathrm{h}} + \alpha_{\mathrm{c}}$, $\alpha_2 = \alpha_{\mathrm{c}}$, $\alpha_3 = \alpha_{\mathrm{h}}$ based on the ATES well states and ATES pump flow direction. These different operating modes were introduced by piecewise affine (PWA) system (2-16). We must note that we do not have to incorporate these different power coefficients

into the ATES system dynamics (2-11), because the ATES states will be reset to zero each time the state reaches negative values. First let us define the vector of auxiliary variables:

$$\boldsymbol{z}_{\mathrm{a}}(k) := \begin{bmatrix} \alpha_1 & 0 & 0 \\ 0 & \alpha_2 & 0 \\ 0 & 0 & \alpha_3 \end{bmatrix} \boldsymbol{\delta}_{\mathrm{a}}(k) u_{\mathrm{a}}(k), \tag{A-1}$$

where $\boldsymbol{z}_{\mathrm{a}} \in \mathbb{R}^3$ contains the auxiliary variables and $\boldsymbol{\delta}_{\mathrm{a}} \in \mathbb{R}^3$ denotes the vector of binary variables. Furthermore, resorting to HYSDEL [40], the auxiliary binary vector $\boldsymbol{b}_{\mathrm{a}} \in \mathbb{R}^4$ is introduced to incorporate the logic. Now the MLD system model of the district heating system is given by:

$$\boldsymbol{x}_{\mathrm{a}}(k+1) = \boldsymbol{A}_{\mathrm{a}}(k)\boldsymbol{x}_{\mathrm{a}}(k) + \boldsymbol{B}_{\mathrm{a}}(k)u_{\mathrm{a}}(k)\tau, \tag{A-2}$$

$$Q_{\mathrm{hp}}(k) = \boldsymbol{D}_{\mathrm{a}}\boldsymbol{z}_{\mathrm{a}}(k) + Q_{\mathrm{d}}(k), \tag{A-3}$$

$$\boldsymbol{E}_{\mathrm{a1}}\boldsymbol{x}_{\mathrm{a}}(k) + \boldsymbol{E}_{\mathrm{a2}}u_{\mathrm{a}}(k)\tau + \boldsymbol{E}_{\mathrm{a3}}\boldsymbol{z}_{\mathrm{a}}(k) + \boldsymbol{E}_{\mathrm{a4}}\boldsymbol{\delta}_{\mathrm{a}}(k) + \boldsymbol{E}_{\mathrm{a5}}\boldsymbol{b}_{\mathrm{a}}(k) \leq \boldsymbol{E}_{\mathrm{aff}}, \tag{A-4}$$

where, $\boldsymbol{x}_{\mathrm{a}}(k) = \begin{bmatrix} S_{\mathrm{h}}(k) & S_{\mathrm{c}}(k) \end{bmatrix}^T \in \mathbb{R}^2$ and $u_{\mathrm{a}}(k) \in \mathbb{R}$ are the state vector and input, respectively. Let us first introduce the notation of the zero matrix with n columns and m rows $\mathbf{0}_{n,m}$ as a matrix whose entities are zero. Now, the MLD system matrices are:

$$\boldsymbol{D}_{\mathrm{a}} = \begin{bmatrix} 1 & 1 & 1 \end{bmatrix}, \qquad \boldsymbol{E}_{\mathrm{a1}} = \begin{bmatrix} \mathbf{0}_{1,8} & 1 & -1 & -1 & 1 & \mathbf{0}_{1,24} \\ \mathbf{0}_{1,8} & -1 & 1 & 1 & -1 & \mathbf{0}_{1,24} \end{bmatrix}^T,$$

$$\boldsymbol{E}_{\mathrm{a2}} = \begin{bmatrix} \mathbf{0}_{1,12} & 1 & -1 & -1 & 1 & \mathbf{0}_{1,8} & \alpha_1 & -\alpha_1 & 0 & 0 \\ & & & & & & \alpha_2 & -\alpha_2 & 0 & 0 & \alpha_3 & -\alpha_3 \end{bmatrix}^T,$$

$$\boldsymbol{E}_{\mathrm{a3}} = \begin{bmatrix} \mathbf{0}_{1,2} & -1 & 1 & \mathbf{0}_{1,20} & -1 & 1 & -1 & 1 & \mathbf{0}_{1,8} \\ \mathbf{0}_{1,4} & -1 & 1 & \mathbf{0}_{1,22} & -1 & 1 & -1 & 1 & \mathbf{0}_{1,4} \\ \mathbf{0}_{1,6} & -1 & 1 & \mathbf{0}_{1,25} & 0 & -1 & 1 & -1 & 1 \end{bmatrix}^T$$

$$\boldsymbol{E}_{\mathrm{a4}} = \begin{bmatrix} -1 & 1 & \mathbf{0}_{1,14} & -1 & 1 & \mathbf{0}_{1,6} & u_{\mathrm{a}}^{\max}(\alpha_1+\alpha_2) \\ \mathbf{0}_{1,18} & -1 & 1 & 1 & \mathbf{0}_{1,7} & u_{\mathrm{a}}^{\max}(\alpha_2+\alpha_3) & -u_{\mathrm{a}}^{\min}(\alpha_2+\alpha_3) \\ \mathbf{0}_{1,21} & -1 & 1 & 1 & \mathbf{0}_{1,6} & 0 & 0 \end{bmatrix}$$

$$\begin{bmatrix} -u_{\mathrm{a}}^{\min}(\alpha_1+\alpha_2) & u_{\mathrm{a}}^{\min}(\alpha_1+\alpha_2) & -u_{\mathrm{a}}^{\max}(\alpha_1+\alpha_2) & \mathbf{0}_{1,8} \\ u_{\mathrm{a}}^{\max}(\alpha_2+\alpha_3) & -u_{\mathrm{a}}^{\min}(\alpha_2+\alpha_3) & \mathbf{0}_{1,3} & 0 \\ u_{\mathrm{a}}^{\min}(\alpha_1+\alpha_3) & -u_{\mathrm{a}}^{\max}(\alpha_1+\alpha_3) & u_{\mathrm{a}}^{\min}(\alpha_1+\alpha_3) & -u_{\mathrm{a}}^{\max}(\alpha_1+\alpha_3) \end{bmatrix}^T$$

$$\boldsymbol{E}_{\mathrm{a5}} = \begin{bmatrix} \mathbf{0}_{1,8} & -x_{\mathrm{a}}^{\max}+\epsilon & x_{\mathrm{a}}^{\min}-\epsilon & \mathbf{0}_{1,6} & 1 & -1 & \mathbf{0}_{1,18} \\ \mathbf{0}_{1,10} & x_{\mathrm{a}}^{\min}-\epsilon & x_{\mathrm{a}}^{\max}+\epsilon & \mathbf{0}_{1,6} & 1 & -1 & \mathbf{0}_{1,16} \\ \mathbf{0}_{1,12} & u_{\mathrm{a}}^{\min}-\epsilon & u_{\mathrm{a}}^{\max}+\epsilon & 1 & 0 & -1 & \mathbf{0}_{1,19} \\ \mathbf{0}_{1,14} & u_{\mathrm{a}}^{\min}-\epsilon & u_{\mathrm{a}}^{\max}+\epsilon & 0 & 0 & 0 & \mathbf{0}_{1,19} \end{bmatrix}^T,$$

$$\boldsymbol{E}_{\mathrm{aff}} = \begin{bmatrix} 0 & 1 & -u_{\mathrm{a}}^{\min}(\alpha_1+\alpha_2) & u_{\mathrm{a}}^{\max}(\alpha_1+\alpha_2) & -u_{\mathrm{a}}^{\min}(\alpha_2+\alpha_3) & u_{\mathrm{a}}^{\max}(\alpha_2+\alpha_3) \\ -u_{\mathrm{a}}^{\min}(\alpha_1+\alpha_3) & u_{\mathrm{a}}^{\max}(\alpha_1+\alpha_3) & -\epsilon & -x_{\mathrm{a}}^{\min} & -\epsilon & x_{\mathrm{a}}^{\max} & -\epsilon & u_{\mathrm{a}}^{\max} & -\epsilon & u_{\mathrm{a}}^{\max} \\ 0 & 0 & 1 & 0 & 0 & 1 & 0 & 0 & u_{\mathrm{a}}^{\max}(\alpha_1+\alpha_2) & \\ -u_{\mathrm{a}}^{\min}(\alpha_1+\alpha_2) & 0 & 0 & u_{\mathrm{a}}^{\max}(\alpha_1+\alpha_3) & u_{\mathrm{a}}^{\min}(\alpha_1+\alpha_3) & 0 & 0 \end{bmatrix}^T$$

A-3 Overall System Matrices

The system matrices of the overall system MLD model (2-30) are given by:

$$\boldsymbol{A} = \begin{bmatrix} \eta_{\text{b1}} & 0 & 0 & 0 \\ 0 & \boldsymbol{A}_{\text{a}} & 0 & 0 \\ 0 & 0 & 1 & 0 \\ 0 & 0 & 0 & 1 \end{bmatrix}, \quad \boldsymbol{B_1} = \begin{bmatrix} \eta_{\text{dch}} & -\frac{\eta_{\text{dch}}}{\text{COP}(k)} & \eta_{\text{dch}}\eta_{\text{el,dw}} & \frac{\eta_{\text{dch}}}{\eta_{\text{hy,el}}} & 0 & 0 \\ \boldsymbol{0}_{2,1} & \boldsymbol{0}_{2,1} & \boldsymbol{0}_{2,1} & \boldsymbol{0}_{2,1} & \boldsymbol{0}_{2,1} & \boldsymbol{B}_{\text{a}} \\ 0 & 0 & 0 & 1 & 1 & 0 \\ 0 & 0 & 0 & \eta_{\text{dw,hy}} & 0 & 1 \end{bmatrix},$$

$$\boldsymbol{B_2} = \begin{bmatrix} -(\eta_{\text{dch}} - \eta_{\text{ch}}) & \boldsymbol{0}_{1,3} \\ \boldsymbol{0}_{2,1} & \boldsymbol{0}_{2,3} \\ 0 & \boldsymbol{0}_{1,3} \\ 0 & \boldsymbol{0}_{1,3} \end{bmatrix}, \quad \boldsymbol{B_3} = \begin{bmatrix} 1 & 0 & 0 & 0 & 0 \\ \boldsymbol{0}_{2,1} & \boldsymbol{0}_{2,1} & \boldsymbol{0}_{2,1} & \boldsymbol{0}_{2,1} & \boldsymbol{0}_{2,1} \\ 0 & 0 & 0 & -1 & 0 \\ 0 & 0 & 0 & 0 & -1 \end{bmatrix},$$

$$\boldsymbol{E_1} = \begin{bmatrix} \boldsymbol{0}_{6,1} & \boldsymbol{0}_{6,2} & \boldsymbol{0}_{6,1} & \boldsymbol{0}_{6,1} \\ \boldsymbol{0}_{36,1} & \boldsymbol{E}_{\text{a1}} & \boldsymbol{0}_{36,1} & \boldsymbol{0}_{36,1} \end{bmatrix}, \boldsymbol{E_2} = \begin{bmatrix} \boldsymbol{0}_{6,1} & \boldsymbol{0}_{6,2} & \boldsymbol{0}_{6,1} & \boldsymbol{0}_{6,1} & \boldsymbol{0}_{6,1} & \boldsymbol{0}_{6,1} \\ \boldsymbol{0}_{36,1} & \boldsymbol{E}_{\text{a2}} & \boldsymbol{0}_{36,1} & \boldsymbol{0}_{36,1} & \boldsymbol{0}_{36,1} & \boldsymbol{0}_{36,1} \end{bmatrix}$$

$$\boldsymbol{E_3} = \begin{bmatrix} \boldsymbol{E}_{\text{b1}} & \boldsymbol{0}_{6,3} & \boldsymbol{0}_{6,4} \\ \boldsymbol{0}_{36,1} & \boldsymbol{E}_{\text{a4}} & \boldsymbol{E}_{\text{a5}} \end{bmatrix}, \boldsymbol{E_4} = \begin{bmatrix} \boldsymbol{E}_{\text{b2}} & \boldsymbol{0}_{6,3} \\ \boldsymbol{0}_{36,1} & \boldsymbol{E}_{\text{a3}} \end{bmatrix}$$

$$\boldsymbol{d} = \begin{bmatrix} \boldsymbol{E}_{\text{b4}} \\ \boldsymbol{E}_{\text{aff}} \end{bmatrix}$$

Appendix B

Rule-Based Control Strategy

The Rule-Based Controller (RBC) algorithm is given on the next page.

Algorithm 2: Rule-Based Control

Hydrogen:

if $x_{\mathrm{el}}(k) < H_{\mathrm{d}}^{\max}$ **then**
  $H_{\mathrm{el}}(k) = H_{\mathrm{el}}^{\max}$
else if $x_{\mathrm{el}}(k) + H_{\mathrm{el}}^{\max} < H_{\mathrm{d}}^{\max}$ **then**
  $H_{\mathrm{el}}(k) = H_{\mathrm{el}}^{\max}$
  $H_{\mathrm{trade}}(k) = H_{\mathrm{trade}}^{\max}$
else
  $H_{\mathrm{el}}(k) = 0$
  $H_{\mathrm{trade}}(k) = 0$
end

Demineralised Water:

if $x_{\mathrm{dw}}(k) - \eta_{\mathrm{dw,el}} H_{\mathrm{el}}(k) < F_{\mathrm{d}}^{\max}$ **then**
  $F_{\mathrm{ro}}(k) = F_{\mathrm{ro}}^{\max}$
else
  $F_{\mathrm{ro}} = 0$
end

District Heating System:

if $E_{\mathrm{pv}}(k) - P_{\mathrm{el}}(k) - P_{\mathrm{ro}}(k) > P_{\mathrm{hp}}^{\max}$ **then**
  $P_{\mathrm{hp}}(k) = P_{\mathrm{hp}}^{\max}$
else
  $P_{\mathrm{hp}}(k) = E_{\mathrm{pv}}(k) - P_{\mathrm{el}}(k) - P_{\mathrm{ro}}(k)$
end

Microgrid:

if $E_{\mathrm{pv}}(k) - P_{\mathrm{el}}(k) - P_{\mathrm{ro}}(k) - P_{\mathrm{hp}}(k) > P_{\mathrm{b}}^{\max}$ **then**
  if $x_{\mathrm{b}}(k) + P_{\mathrm{b}}^{\max} > x_{\mathrm{b}}^{\max}$ **then**
    $P_{\mathrm{b}}(k) = (x_{\mathrm{b}}^{\max} - x_{\mathrm{b}}(k))$
    $P_{\mathrm{grid}}(k) = E_{\mathrm{pv}}(k) - P_{\mathrm{el}}(k) - P_{\mathrm{ro}}(k) - P_{\mathrm{hp}}(k) - P_{\mathrm{b}}(k)$
  else
    $P_{\mathrm{b}}(k) = E_{\mathrm{pv}}(k) - P_{\mathrm{el}}(k) - P_{\mathrm{ro}}(k) - P_{\mathrm{hp}}(k)$
  end
else
  if $x_{\mathrm{b}}(k) + E_{\mathrm{pv}}(k) - P_{\mathrm{el}}(k) - P_{\mathrm{ro}}(k) - P_{\mathrm{hp}}(k) > x_{\mathrm{b}}^{\max}$ **then**
    $P_{\mathrm{b}}(k) = (x_{\mathrm{b}}^{\max} - x_{\mathrm{b}}(k))$
    $P_{\mathrm{grid}}(k) = E_{\mathrm{pv}}(k) - P_{\mathrm{el}}(k) - P_{\mathrm{ro}}(k) - P_{\mathrm{hp}}(k) - P_{\mathrm{b}}(k)$
  else
    $P_{\mathrm{b}}(k) = E_{\mathrm{pv}}(k) - P_{\mathrm{el}}(k) - P_{\mathrm{ro}}(k) - P_{\mathrm{hp}}(k)$
  end
end

Bibliography

[1] "Paris Agreement." UNTC XXVII 7.d.

[2] M. Rutte, S. van Haersma Buma, A. Pechtold, and G.-J. Segers, "Vertrouwen in de toekomst." https://www.kabinetsformatie2017.nl/binaries/kabinetsformatie/documenten/publicaties/2017/10/10/regeerakkoord-vertrouwen-in-de-toekomst/Regeerakkoord+2017-2021.pdf, 2017.

[3] "Distributed Generation Growing More Popular." https://share.america.gov/distributed-generation-growing-more-popular/. Accessed: 2019-11-15.

[4] M. A. Müller, *Distributed and economic model predictive control: beyond setpoint stabilization*. Logos Verlag Berlin GmbH, 2014.

[5] F. Graaf de, "New Strategies For Smart Integrated Decentralised Energy Systems." https://www.metabolic.nl/publications/side-systems/, 2018.

[6] J. Starn, "Germany set to pay customers for electricity usage as renewable energy generation creates huge power surplus." https://www.independent.co.uk/environment/germany-grids-paying-electricity-customers-renewable-energy-power-surplus-wind-solar-generation-a8022576.html, *Independent*, 2017.

[7] H. Lund and E. Münster, "Management of surplus electricity-production from a fluctuating renewable-energy source," *Applied Energy*, vol. 76, no. 1, pp. 65 – 74, 2003. Energex 2002 - Energy Policies and Economics and Rational Use of Energy of Energy Topics VI and VII.

[8] H. Santen, "Nieuwe lijn brengt Duitse windstroom het land binnen." https://www.nrc.nl/nieuws/2018/09/25/nieuwe-lijn-brengt-duitse-windstroom-het-land-binnen-a1775817, *nrc.nl*, 2018.

[9] P. D. Lund, J. Lindgren, J. Mikkola, and J. Salpakari, "Review of energy system flexibility measures to enable high levels of variable renewable electricity," *Renewable and Sustainable Energy Reviews*, vol. 45, pp. 785 – 807, 2015.

[10] P. Mancarella, "MES (multi-energy systems): An overview of concepts and evaluation models," *Energy*, vol. 65, pp. 1 – 17, 2014.

[11] M. Geidl, *Integrated modeling and optimization of multi-carrier energy systems*. PhD thesis, ETH Zurich, 2007.

[12] G. Chicco and P. Mancarella, "Distributed multi-generation: A comprehensive view," *Renewable and Sustainable Energy Reviews*, vol. 13, no. 3, pp. 535 – 551, 2009.

[13] M. A. Bucher, T. W. Haring, F. Bosshard, and G. Andersson, "Modeling and economic evaluation of Power2Gas technology using energy hub concept," in *2015 IEEE Power Energy Society General Meeting*, pp. 1–5, 2015.

[14] D. I. H. Rodriguez, J. Hinker, and J. M. A. Myrzik, "On the problem formulation of model predictive control for demand response of a power-to-heat home microgrid," in *2016 Power Systems Computation Conference (PSCC)*, pp. 1–8, 2016.

[15] C. Fu, J. Lin, Y. Song, Y. Zhou, and S. Mu, "Model predictive control of an integrated energy microgrid combining power to heat and hydrogen," in *2017 IEEE Conference on Energy Internet and Energy System Integration (EI2)*, pp. 1–6, 2017.

[16] J. Allegrini, K. Orehounig, G. Mavromatidis, F. Ruesch, V. Dorer, and R. Evins, "A review of modelling approaches and tools for the simulation of district-scale energy systems," *Renewable and Sustainable Energy Reviews*, vol. 52, pp. 1391 – 1404, 2015.

[17] C. Baumann, R. Schuster, and A. Moser, "Economic potential of power-to-gas energy storages," in *2013 10th International Conference on the European Energy Market (EEM)*, pp. 1–6, 2013.

[18] S. Clegg and P. Mancarella, "Integrated Modeling and Assessment of the Operational Impact of Power-to-Gas (P2G) on Electrical and Gas Transmission Networks," *IEEE Transactions on Sustainable Energy*, vol. 6, no. 4, pp. 1234–1244, 2015.

[19] R. R. Dickinson, N. Lymperopoulos, A. Le Duigou, P. Lucchese, C. Mansilla, O. Tlili, N. J. Samsatli, S. Samsatli, M. Weeda, D. Thomas, P. Mancarella, F. Dolci, and E. Weidner, "Power-to-hydrogen and hydrogen-to-X pathways: Opportunities for next generation energy systems," in *2017 14th International Conference on the European Energy Market (EEM)*, pp. 1–6, 2017.

[20] W. Kempton and J. Tomić, "Vehicle-to-grid power implementation: From stabilizing the grid to supporting large-scale renewable energy," *Journal of Power Sources*, vol. 144, pp. 280–294, 2005.

[21] F. Alavi, E. P. Lee, N. van de Wouw, B. D. Schutter, and Z. Lukszo, "Fuel cell cars in a microgrid for synergies between hydrogen and electricity networks," *Applied Energy*, vol. 192, pp. 296 – 304, 2017.

[22] E. F. Camacho, C. Bordons, and C. B. Alba, *Model Predictive Control*. Springer London, 2007.

[23] V. Rostampour and T. Keviczky, "Probabilistic energy management for building climate comfort in smart thermal grids with seasonal storage systems," *IEEE Transactions on Smart Grid*, vol. 10, no. 4, pp. 3687–3697, 2018.

[24] P. D. Christofides, R. Scattolini, D. M. de la Peña, and J. Liu, "Distributed model predictive control: A tutorial review and future research directions," *Computers Chemical Engineering*, vol. 51, pp. 21 – 41, 2013. CPC VIII.

[25] S. R. Cominesi, M. Farina, L. Giulioni, B. Picasso, and R. Scattolini, "A two-layer stochastic model predictive control scheme for microgrids," *IEEE Transactions on Control Systems Technology*, vol. 26, no. 1, pp. 1–13, 2017.

[26] F. Oldewurtel, A. Parisio, C. N. Jones, D. Gyalistras, M. Gwerder, V. Stauch, B. Lehmann, and M. Morari, "Use of model predictive control and weather forecasts for energy efficient building climate control," *Energy and Buildings*, vol. 45, pp. 15 – 27, 2012.

[27] A. Parisio, C. Wiezorek, T. Kyntäjä, J. Elo, K. Strunz, and K. H. Johansson, "Cooperative MPC-Based Energy Management for Networked Microgrids," *IEEE Transactions on Smart Grid*, vol. 8, no. 6, pp. 3066–3074, 2017.

[28] A. Parisio, E. Rikos, and L. Glielmo, "A Model Predictive Control Approach to Microgrid Operation Optimization," *IEEE Transactions on Control Systems Technology*, vol. 22, no. 5, pp. 1813–1827, 2014.

[29] R. Halvgaard, N. K. Poulsen, H. Madsen, and J. B. Jorgensen, "Economic Model Predictive Control for building climate control in a Smart Grid," in *2012 IEEE PES Innovative Smart Grid Technologies (ISGT)*, pp. 1–6, 2012.

[30] A. van Wijk, E. van der Roest, and J. Boere, "SOLAR POWER TO THE PEOPLE." https://www.kwrwater.nl/wp-content/uploads/2017/11/Solar-Power-to-the-People-NL.pdf, Allied Waters, 2017.

[31] M. Branicky, V. Borkar, and S. Mitter, "A Unified Framework for Hybrid Control: Model and Optimal Control Theory," *Automatic Control, IEEE Transactions on*, vol. 43, pp. 31–45, 1998.

[32] E. Sontag, "Nonlinear Regulation: The Piecewise Linear Approach," *Automatic Control, IEEE Transactions on*, vol. 26, pp. 346 – 358, 1981.

[33] A. Bemporad and M. Morari, "Control of systems integrating logic, dynamics, and constraints," *Automatica*, vol. 35, no. 3, pp. 407 – 427, 1999.

[34] J. M. Schumacher, S. Weiland, and W. P. M. H. Heemels, "Linear Complementarity Systems," *SIAM Journal of Applied Mathematics*, vol. 60, pp. 1234–1269, 2000.

[35] M. Johansson and A. Rantzer, "Computation of piecewise quadratic Lyapunov functions for hybrid systems," *IEEE Transactions on Automatic Control*, vol. 43, no. 4, pp. 555–559, 1998.

[36] W. Heemels, B. D. Schutter, and A. Bemporad, "Equivalence of hybrid dynamical models," *Automatica*, vol. 37, no. 7, pp. 1085 – 1091, 2001.

[37] A. Parisio and L. Glielmo, "Stochastic model predictive control for economic/environmental operation management of microgrids," in *Control Conference (ECC), 2013 European*, pp. 2014–2019, IEEE, 2013.

[38] W. Sommer, J. Valstar, I. Leusbrock, T. Grotenhuis, and H. Rijnaarts, "Optimization and spatial pattern of large-scale aquifer thermal energy storage," *Applied Energy*, vol. 137, pp. 322 – 337, 2015.

[39] V. Rostampour and T. Keviczky, "Energy Management for Building Climate Comfort in Uncertain Smart Thermal Grids with Aquifer Thermal Energy Storage," *IFAC-PapersOnLine*, vol. 50, no. 1, pp. 13156 – 13163, 2017. 20th IFAC World Congress.

[40] F. D. Torrisi and A. Bemporad, "HYSDEL-a tool for generating computational hybrid models for analysis and synthesis problems," *IEEE Transactions on Control Systems Technology*, vol. 12, no. 2, pp. 235–249, 2004.

[41] T. Hong and S. Fan, "Probabilistic electric load forecasting: A tutorial review," *International Journal of Forecasting*, vol. 32, no. 3, pp. 914–938, 2016.

[42] L. Hernandez, C. Baladron, J. M. Aguiar, B. Carro, A. J. Sanchez-Esguevillas, J. Lloret, and J. Massana, "A Survey on Electric Power Demand Forecasting: Future Trends in Smart Grids, Microgrids and Smart Buildings," *IEEE Communications Surveys Tutorials*, vol. 16, no. 3, pp. 1460–1495, 2014.

[43] J. Antonanzas, N. Osorio, R. Escobar, R. Urraca, F. M. de Pison, and F. Antonanzas-Torres, "Review of photovoltaic power forecasting," *Solar Energy*, vol. 136, pp. 78 – 111, 2016.

[44] R. R. Negenborn, *Multi-agent model predictive control with applications to power networks*. PhD thesis, TU Delft, 2007.

[45] J. B. Rawlings, D. Angeli, and C. N. Bates, "Fundamentals of economic model predictive control.," in *CDC*, pp. 3851–3861, 2012.

[46] I. Sarantis, F. Alavi, and B. De Schutter, "Optimal power scheduling of fuel-cell-car-based microgrids," in *2017 IEEE 56th Annual Conference on Decision and Control (CDC)*, pp. 5062–5067, 2017.

[47] M. Arnold and G. Andersson, "Model predictive control of energy storage including uncertain forecasts," in *Power Systems Computation Conference (PSCC), Stockholm, Sweden*, vol. 23, pp. 24–29, 2011.

[48] M. Petrollese, L. Valverde, D. Cocco, G. Cau, and J. Guerra, "Real-time integration of optimal generation scheduling with MPC for the energy management of a renewable hydrogen-based microgrid," *Applied Energy*, vol. 166, pp. 96 – 106, 2016.

[49] A. Bemporad, "Model Predictive Control - Stochastic MPC." Lecture Model Predictive Control http://cse.lab.imtlucca.it/~bemporad/teaching/mpc/imt/7-stochastic_mpc.pdf, IMT School for Advanced Studies Lucca, 2019.

[50] P. Tatjewski, "Advanced control and on-line process optimization in multilayer structures," *Annual Reviews in Control*, vol. 32, no. 1, pp. 71 – 85, 2008.

[51] D. Barcelliy, A. Bemporad, and G. Ripaccioliy, "Hierarchical multi-rate control design for constrained linear systems," in *49th IEEE Conference on Decision and Control (CDC)*, pp. 5216–5221, 2010.

[52] A. Bemporad, C. Pascucci, and C. Rocchi, "Hierarchical and Hybrid Model Predictive Control of Quadcopter Air Vehicles," *IFAC Proceedings Volumes*, vol. 42, no. 17, pp. 14 – 19, 2009. 3rd IFAC Conference on Analysis and Design of Hybrid Systems.

[53] M. Joševski and D. Abel, "Multi-time scale model predictive control framework for energy management of hybrid electric vehicles," in *53rd IEEE Conference on Decision and Control*, pp. 2523–2528, IEEE, 2014.

[54] M. Farina, L. Giulioni, and R. Scattolini, "Stochastic linear Model Predictive Control with chance constraints - A review," *Journal of Process Control*, vol. 44, pp. 53 – 67, 2016.

[55] A. Parisio, D. Varagnolo, M. Molinari, G. Pattarello, L. Fabietti, and K. H. Johansson, "Implementation of a Scenario-based MPC for HVAC Systems: an Experimental Case Study," *IFAC Proceedings Volumes*, vol. 47, no. 3, pp. 599 – 605, 2014. 19th IFAC World Congress.

[56] J. Löfberg, "YALMIP : A Toolbox for Modeling and Optimization in MATLAB," in *In Proceedings of the CACSD Conference*, (Taipei, Taiwan), 2004.

Glossary

List of Acronyms

ATES	Aquifer Thermal Energy Storage
BESS	battery energy storage system
COP	Coefficient of Performance
CEMPC	certainty-equivalent MPC
EMS	Energy Management System
ESEP	exportable surplus electricity production
HiMPC	Hierarchical Model Predictive Control
HMPC	Heuristic Model Predictive Control
LC	linear complementarity
LL-MPC	lower-layer MPC
MES	Multi-Energy System
MILP	Mixed Integer Linear Programming
MIQP	Mixed Integer Quadratic Programming
MLD	Mixed Logical Dynamical
MPC	Model Predictive Control
PCC	Point of Common Coupling
PMPC	prescient MPC
PV	photovoltaic
PWA	piecewise affine

RBC Rule-Based Controller

RES Renewable Energy Source

SEP surplus electricity production

SMPC stochastic MPC

SoC state of charge

UL-MPC upper-layer MPC

List of Symbols

T	Transpose of a vector
h	Variables related to the Heuristic MPC optimal control problem
l	Variables related to the Hierarchical MPC's lower-layer optimal control problem
max	Maximum value of a variable
min	Minimum value of a variable
u	Variables related to the Hierarchical MPC's upper-layer optimal control problem
α	Power coefficient of water
δ	Binary input
η	Efficiency
γ	Persistence model lag
κ	Heuristic MPC tuning variable denoting the number of months ahead when heat is going to be used
λ	Heuristic MPC tuning variable representing the greediness of heat storage depletion
$\mathbb{R}$	Set of real numbers
$\mathbb{U}$	Set of feasible inputs
$\mathbb{W}$	Set containing disturbance vector
$\mathbb{X}$	Set of feasible states
$\mathbb{Z}$	Set of integer numbers
$\mathbb{Z}_{\geq a}$	Set of integer numbers greater than or equal to $a \in \mathbb{R}$
ω	Disturbance
ψ	Heuristic MPC tuning variable for determining the start of heat production
ρ	Slack variable
τ	Sampling time
COP	Coefficient of Performance, the efficiency of a heat pump
C	Cost of interaction with an external party
E	Electrical Energy
$E[\cdot]$	Expectation operator
F	Volume of demineralised water
H	Amount of hydrogen
J	MPC cost function over the prediction horizon
l	Stage cost function
N	Prediction Horizon
N_{s}	Number of scenario realisations
P	Power
$P[\cdot]$	Probability operator
Q	Thermal Energy
u	Input

v	Decision variable
V_f	Terminal cost function
x	State
z	Auxiliary variable introduced by MLD modelling framework
$[a, b]$	Interval $\{y \in \mathbb{R} : a \leq y \leq b\}$ for constants $a, b \in \mathbb{R}$